HCCI and SICI combustion modes analysis with simultaneous PLIF imaging of formaldehyde and high-speed chemiluminescence in a rapid compression machine

Camille Strozzi, Alain Claverie, Vivien Prevost, Julien Sotton, Marc Bellenoue

HCCI and SICI combustion modes analysis with simultaneous PLIF imaging of formaldehyde and high-speed chemiluminescence in a Rapid Compression Machine

Camille Strozzi*[1], Alain Claverie[2], Vivien Prevost[2], Julien Sotton[2], Marc Bellenoue[2]

[1] Institut Pprime, CNRS, Université de Poitiers, ISAE-ENSMA, F-86962 Futuroscope Chasseneuil, France

[2] Institut Pprime, CNRS, ISAE-ENSMA, Université de Poitiers, F-86962 Futuroscope Chasseneuil, France

* corresponding author: camille.strozzi@ensma.fr

Submitted to Combustion and Flame as a **Full Length article**.
Shortened running title: HCCI/SICI analysis by PLIF/chemiluminescence.
Keywords: RCM, cool flame, autoignition fronts, PLIF, HCCI, SICI.

Abstract: Homogeneous Charge Compression Ignition (HCCI) and Spark Induced Compression Ignition (SICI) of a lean iso-octane air mixture are investigated through simultaneous measurements of planar laser-induced fluorescence at 355 nm and high-speed chemiluminescence in the parallelepipedic combustion vessel of a rapid compression machine (RCM). A radiofrequency igniter with a high energy deposit (305 mJ) is used to investigate the SICI combustion phenomena in lean conditions ($\Phi = 0.5$), relatively close to the frontiers of the SICI regime. Fluorescence images enable to monitor both the development of the cool flame process and the topology and dynamics of reaction fronts during the second stage of ignition. The results are first analyzed from a phenomenological point of view, bringing insights into the understanding of the both HCCI and SICI combustion processes as they take place in the RCM. Additional data are gathered from double-pulse 355 nm PLIF imaging, with focus on the temporal evolution of the cool flame and on the reaction front propagation during hot ignition. From a more quantitative point of view, an analysis of apparent velocities of the reaction zones is then presented, and large variations of these values are observed depending on the experimental conditions. These local quantities are closely related to the global heat release rate which is a key parameter for practical applications of HCCI and SICI combustion modes. The proposed simultaneous diagnostics finally lead to a better understanding in the local reaction modes, namely deflagration, spontaneous ignition fronts and bulk auto-ignition – e.g. volumetric auto-ignition - , which are implied in the combustion processes. The results highlight the complex aerothermal interactions taking place in the RCM vessel, in particular through the pre-ignition thermal stratification. The results suggest the latter strongly affects the HCCI combustion process, but also drives the heat release rate during the second stage of the SICI combustion mode. Furthermore, deflagration fronts are found to be significantly affected by cool flame chemistry, as well as by the large and small scale structures of the fluid flow.

1. Introduction

The Homogeneous Charge Compression Ignition (HCCI) and Spark Induced Compression Ignition (SICI) combustion processes constitute advanced operating modes for automotive engines implying both high thermal efficiency and low NOx and soot emission thanks to the combustion of lean or diluted mixtures featuring a relative homogeneity [1-4]. They are part of the different strategies involved in Low Temperature Combustion (LTC) engines [5], and present as well some similarities with the MILD combustion concept [6]. Spark induced compression ignition (SICI) appears as a relatively new combustion control technology and a promising combustion mode in gasoline engines with high efficiency [7]. Spark assistance operates by initiating a reaction kernel before the main combustion event; the propagating flame then consumes a portion of the charge and releases fuel energy so the remainder of the charge auto-ignites earlier than it would have otherwise. The control of self-ignition mechanisms implied in such operating modes as well as the limitation of the maximum heat release rates constitute major challenges for practical applications to engines.

Rapid Compression Machines (RCM) are relevant devices to study such modes of combustion. Those featuring large optical accesses - like the one used in the present study - provide ideal conditions for studying both aerothermal and combustion processes by means of optical diagnostic methods [8,9,10]. For instance, thermal heterogeneities generated during the compression of inert mixtures were characterized by using Planar Laser Induced Fluorescence (PLIF) measurements on the toluene molecule [9]. The same device was also employed to study HCCI combustion of light [10] or heavier hydrocarbon-air mixtures [11]. Several studies were devoted to the delineation between combustion regimes, called mild and strong ignition, during HCCI combustion in such devices, see for instance [10,12]. These regimes are closely related to the local mode of combustion (e.g. autoignition front or deflagration) [10,12,13], and further distinctions between these regimes were proposed in [14,15], depending on the influence of mixing on the reactivity gradients before auto-ignition. The coexistence of deflagration and auto-ignition is also inherent to SICI combustion mode. In this framework, optical diagnostic methods are specifically developed in the present work

to analyze the HCCI and SICI reactive phenomena from a local point of view.

If knocking combustion was the subject of past RCM studies, this is not the case of SICI combustion. The work of Boumehdi et al. [16] can be cited here, as the authors investigated the effect of nanosecond surface dielectric barrier discharges (SDBD) with different voltages on the auto-ignition of mixtures containing methane and butane in a RCM. In particular, no significant effects of the discharge were reported below a threshold value applied to the high voltage electrode and auto-ignition occurred in these conditions. For higher voltage values, flame propagation was evidenced by the authors, but it did not lead to the auto-ignition of the end gas. Therefore reported combustion mode was probably more representative of SI (Spark Ignition) combustion than SICI. As the combustion mode is different, and since SICI results are provided below with the use of an innovative - high energy – igniter, the present work provides new results and is complementary to the study of Boumehdi et al. [16].

The case of premixed isooctane – air mixtures, which are relevant to both Spark Ignition (SI) and SICI applications, is under consideration here. Self-ignition is achieved in a two-stage process in the investigated conditions. After compression stroke, a first rise in pressure is observed coupled with very low light emission, which can only be observed by using an intensifier device. This cool flame is the prelude to the main stage of combustion, e.g. hot ignition. Considering that (i) the post-compression temperature fields feature heterogeneities and that (ii) self-ignition mechanisms exhibit strong temperature dependence, a better understanding of the various aerothermochemical processes requires multidimensional measurements. Optical diagnostics are employed to this end considering that they must be applicable to the severe conditions reached in the present study, i.e. about 700 K and 2.7 MPa after the end of the compression stroke, before the onset of heat release. Formaldehyde is a combustion intermediate species, which is formed in the first stage of hydrocarbon oxidation. Since formaldehyde is completely consumed during hot ignition, it is well-suited as a tracer species of cool flame regions.

In previous studies, detection of formaldehyde was performed in diffusion flames [17] using laser-induced fluorescence (LIF) by excitation of the strong A-X4_0^1 vibronic band at 355 nm. Brackman

et al. [18] studied the overlap between the laser profile and the absorption lines of formaldehyde, saturation effects and the potential occurrence of laser-induced photochemistry and applied the technique to an internal combustion engine. Collin *et al.* [19] proved its efficiency when detecting formaldehyde emissions at the start of low temperature reactions in an HCCI Engine and enhanced the detection of more formaldehyde as the low temperature reactions progressed. Kim and Gandhi [20] monitored formaldehyde PLIF signal in the case of a light load HCCI combustion with various air-fuel equivalence ratios and found that formaldehyde was uniformly formed within the combustion chamber during the first-stage ignition. In order to characterize the flame structure and its transient behavior, Hultqvist *et al*. [21] used high-speed chemiluminescence imaging enabling time resolved observation of light emissions in an engine where cool flames were found to exist some 20 crank angles degrees before Top Dead Center (TDC) using intensified high-speed camera. Different studies aimed at the simultaneous measurement of formaldehyde and OH signals within HCCI engines, see for instance [19,22,23], where formaldehyde traces cool flame regions while OH traces the principal heat release. It has been shown that OH is strongly correlated to high temperature chemistry of premixed combustion. It is as well detected in the burned gases at high temperatures. One may notice other research works with more academic devices correlated the local heat release rate to the convolution of OH and formaldehyde signals obtained by fluorescence within counterflow premixed laminar flames [23].

In this work, the ignition and combustion phases for both HCCI and SICI modes are investigated with single or double-pulse planar laser-induced fluorescence on formaldehyde combined with chemiluminescence imaging. The first objective is to analyze the phenomenology of HCCI processes in the presence of two stage ignition with a fuel highly resistant to auto-ignition, in complement to previous works [24,11]. The second objective is to investigate SICI combustion mode in severe conditions, e.g. close to the limits of existence of this mode. A very lean mixture and a high energy igniter are used for this purpose. The aim is to analyze the topology and dynamics of reaction fronts, as they are closely connected to the heat release rate. The results are part of an experimental database devoted to HCCI/SICI combustion and may be useful for the

assessment of combustion models used in numerical simulations.

The study focuses firstly on phenomenological aspects with the prospect of complementary information from both diagnostics performed from early to late stages of the both HCCI and SICI combustion processes. Instantaneous 2D distribution of formaldehyde is compared with corresponding integrated chemiluminescence signal. The first one is necessary to analyze the end of the combustion process, while chemiluminescence is found particularly efficient to monitor the onset of high temperature reactions. The phenomena are analyzed at the light of velocity and temperature measurements reported in a previous study. In a second phase, a more quantitative approach is considered through the estimation of apparent velocities of reactive fronts.

2. Experimental setup and associated diagnostics

2.1 The Rapid Compression Machine

Experiments are performed within a RCM facility developed in Poitiers [24]. It is designed to cover a wide range of pressure and temperature conditions at top dead center (TDC), including those representative of automotive engines. This can be achieved, for instance, by varying thermodynamic conditions at TDC, the diluent gas composition or the volumetric compression ratio. The latter is set to 12.5 in the present work. The upper part of the combustion chamber can be fitted either with opaque walls or with optical windows. Specifically designed for this purpose, the flat piston has a square cross section with rounded corners (50 x 50 mm, r = 3.6 mm). This shape enables a full optical access to the parallelepipedic dead volume, along a direction normal to the cylinder axis. From a practical point of view, compression of about one liter of reactive mixture is performed in 39 ms. The piston travel is stopped after this stage. As the compression stroke equals 420 mm, the available visualization zone is particularly wide at TDC (~37*50 mm^2). This provides ideal conditions for studying the combustion process by means of optical diagnostic methods.

The following equipment is employed: Initial pressure is measured with an MKS Baratron 220DA pressure transducer with one millibar accuracy. Temperature of the wall is measured by a K-thermocouple. During compression experiments, pressure evolution is followed by a Kistler

601A piezoelectric transducer, coupled to a Kistler 5011B10 charge amplifier in the so-called configuration A, detailed in § 2.2. A Kistler 6125CU20 piezoelectric sensor coupled to a 5018A amplifier are employed in configuration B. Pressure signal is sampled at a frequency of 100 kHz. More details about the RCM and associated measurement sensors can be found in Refs. [10,24].

In the case of SICI operating mode, a radiofrequency (RF) discharge device is set on the cylinder head, generating relatively large volume non-equilibrium plasma. A driver provides an alternative voltage with peak values of 150 V at high frequency to the spark plug, made of a single electrode insulated by from the rest of the chamber. It operates as a second order resonator with a high quality factor ($90 < Q < 100$). Finally the extremity of the electrode delivers a strong local electrical field through a 5 MHz alternative voltage with 10 kV amplitude. The setup integrates a Hall effect probe to measure the current delivered by the driver to the spark plug, and to estimate power delivered at the electrode, see Prevost [25] for more details. In the present study, the energy value provided to the electrode is chosen as follows: by varying gradually the discharge duration or the driver voltage, a decrease in energy level from 305 to 50 mJ is obtained, which leads to a 50% increase in auto-ignition delay values in SICI operation. Conversely, increasing energy levels from 305 mJ to 650 mJ does not affect the auto-ignition instant. That is the reason why 305 mJ is chosen as an optimal value for the present work. It corresponds to a duration of 1 ms for the energy deposit. A good reproducibility is obtained in that case as the maximum deviation in energy is ±5 mJ. The RF discharge system is also chosen as it leads to shorter auto-ignition delays of the end gas in SICI mode in comparison to an arc discharge trigged at the same instant with the same electrical energy: this result was obtained with an automotive spark plug with 1.2 mm gap and long electrodes, e.g. a discharge located at the center of the chamber. In conclusion, the RF system and a deposit of 305 mJ are chosen for the present work as they are found to be optimal to study SICI combustion processes with significant reductions of auto-ignition delays for the very lean mixtures under consideration herein.

2.2 Optical diagnostic methods and associated device

Simultaneous planar laser-induced fluorescence imaging of formaldehyde and high-speed chemiluminescence have been performed in the combustion vessel of the RCM in order to study both the cool flame and hot ignition phenomena, see Fig. 3. Flame propagation is also monitored by broadband chemiluminescence imaging. The simultaneous diagnostics provide complementary information: on the one hand, broadband chemiluminescence images result from the integration of the light emissions along the direction of the chamber depth for visible wavelengths, which enables monitoring the first occurrence of hot ignition whatever its location in the chamber. This diagnostic also features a sufficient acquisition rate to monitor the fast dynamics of the phenomenon. On the other hand, fluorescence images provide more accurate information concerning the shape and location of the reactive front in the visualization plane. Iso-octane – air mixture with a fuel equivalence ratio equal to 0.5 is considered for the experiments. Two optical configurations are employed in the present study.

Configuration A: The experimental setup involves a pulsed Nd-YAG laser (Continuum Surelite II). Detection is ensured by an ICCD camera and a high-speed camera while a semi-transparent mirror enables detection on the same side of the machine (Fig.1). Frequency-tripled laser radiation at 355 nm from the Nd-YAG laser (10 Hz) is used for excitation of formaldehyde with an energy of 90 mJ per pulse released during 5 ns. The laser beam is aligned and directed towards the chamber by a set of mirrors and a combination of spherical and cylindrical lenses generates the divergent laser sheet, with a thickness of approximately 300 µm in the center of the chamber. The resulting 2D fluorescence signal is detected with a Princeton PI-MAX 1K intensified CCD camera (16 bits, 5 Hz) equipped with 105 mm UV Nikon lens and a 03FCG049 filter to remove the elastic contribution of the laser excitation from the fluorescence signal. Detection is then ensured for wavelengths strictly superior to 395 nm. The same approach was followed by Collin *et al.* [19], Brackmann *et al.* [18] and Bladh et al. [55] in engines. Fluorescence spectra clearly evidenced a significant contribution of formaldehyde, but also display a broad structure which origin is not certainly determined. This does not fully exclude the possibility of fluorescence

contributions from other intermediate species formed during the cool flame. In particular, laser induced fluorescence (LIF) of polycyclic aromatic hydrocarbons (PAH) or laser induced incandescence of soot particles (LII) may be excited at 355 nm. However, in diesel spray ignition [26,27], fluorescence emission from PAHs and broadband emissions from soot were observed at locations and instants which are different from that of formaldehyde, the latter being mostly observed close to the injector. PAH fluorescence is more intense than formaldehyde and it occurs in rich combustion regions relatively far from the injector orifice. In that case, heat is released by high temperature reactions. Unlike in the diesel case, PLIF signal is not observed in our experiments during and after the second stage of autoignition, e.g. for high temperature reactions. This confirms the mixture considered here is too lean to produce sufficient amounts of soot and its precursors, and therefore the term formaldehyde PLIF will be employed in the following when exciting at 355 nm. The same approach was reported by Oloffson et al. in a HCCI engine operating in lean conditions [28], and more recently by Tang et al. for a gasoline engine running in partially premixed mode [29].

Fluorescence images reported in the manuscript are processed with a background subtraction and a laser sheet homogeneity correction. Furthermore, noise is attenuated by using an anisotropic filter.

A high-speed camera, Photron SA5 (CMOS, 12 bits, run between 5000 fps and 40000 fps depending on experiments) is placed perpendicularly to the semi-transparent mirror and enables detection of broadband chemiluminescence integrated through the depth of the vessel. The visualization of the whole dead volume is then performed in a direction normal to the cylinder axis with a resolution equal to 656*458 pixels. In the case of SICI combustion, low emission levels are obtained at the beginning of combustion. Therefore a second PI-MAX intensified camera (810*566 pixels) was employed instead of the Photron SA5 for chemiluminescence imaging. A triggering scheme is developed to take into account the different frequencies of lasers and cameras that must synchronize with the RCM operating as a one-shot experiment. A pulse and delay generator is used as a master clock for the PLIF laser operating at 10 Hz for stability purpose. It sends a triggering signal to the intensified camera operating at 5 Hz with 100 ns gate time. The high speed camera and

eventually the RF discharge setup are subsequently triggered by the RCM synchronization box. For each compression experiment with this optical configuration A, a single image for PLIF and an entire high speed video of chemiluminescence are recorded when the Photron SA5 is used.

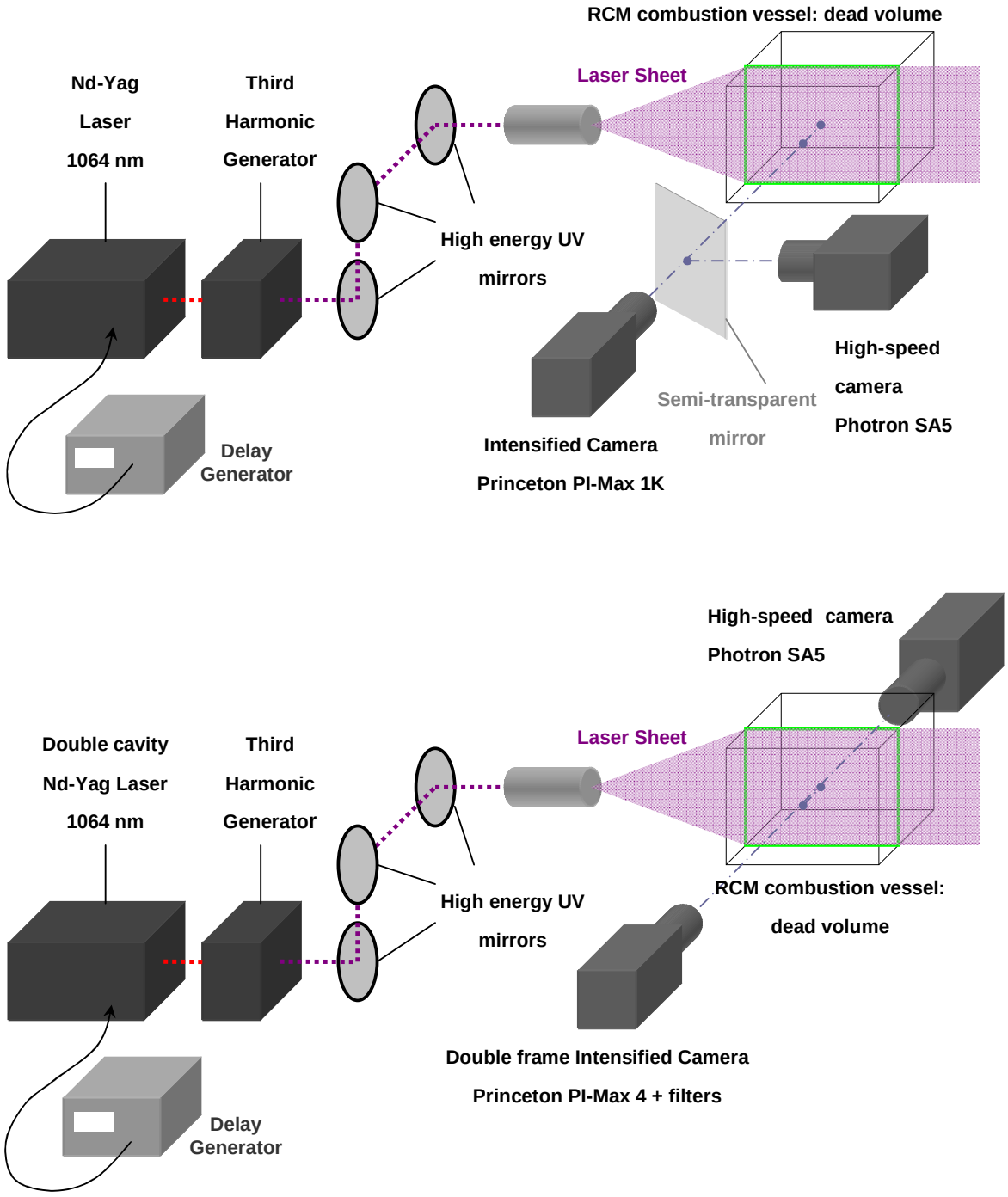

Figure 1: RCM experimental setup for 355 nm PLIF combined with high-speed chemiluminescence, in optical configuration A (Top) and B (Bottom), corresponding respectively to single and double pulse PLIF technique.

Configuration B is employed in a second step. A coupled double-cavity Quantel Brilliant B Nd:YAG laser is employed. It delivers about 120 mJ per pulse at 355 nm, with pairs of pulses delivered at a frequency of 10 Hz. A double frame Princeton PI-MAX4:1024 intensified CCD camera (1024 x 1024 pixels) fitted with a 105 mm Nikon UV lens and a Melles Griot 03FCG049 filter are chosen to record fluorescence emissions of the lean mixture under study. The pairs of images are recorded at 5 Hz. The delay between the images of each pair is constant during an experiment and it varies between 0.1 and 4 ms in the present work. Optical accesses are modified also: the four lateral walls are fitted with quartz windows, so that the intensified camera and the fast camera Photron SA-5 (832x576 pixels and 15000 fps) are recording simultaneously the same combustion process. They are located on both sides of the combustion chamber. For each experiment, both a pair of successive images of fluorescence and a high speed chemiluminescence record are obtained. One may note the beam splitter is removed in comparison to configuration A. Chemiluminescence images obtained from the fast-camera are horizontally reversed for the sake of comparison. This fully optical configuration B also provides a more homogeneous background of the fluorescence images, as pressure sensor and inlet orifice are located in the cylinder head, while they are in the back wall of the chamber in configuration A.

3. Phenomenological analysis of the combustion process

First part of the present work is dedicated to the phenomenological aspects of HCCI and then SICI combustion modes, especially from a local point of view. Both topology and dynamics of the reactive fronts are investigated as they are closely connected to the global heat release rate, which constitutes a key parameter for these combustion modes. Auto-ignition experiments (HCCI) are first considered at two distinct pressure conditions, i.e. about 20 and 27 bar at TDC, corresponding to short and long ignition delay values, see Tab. 1. SICI combustion experiments are then reported. In that case, reactions are initiated during compression stroke using electrical discharge. This leads to a combustion timing similar to that of short ignition delay experiments, which enables a relevant comparison between SICI and HCCI modes.

	HCCI Short ignition delays		SICI	HCCI Long ignition delays
Optical configuration	A	B *- for cool flame -*	A	B
P_{TDC} (bar)	26.9	27.4	20.3	19.6
T_{adc_TDC} (K) - adiabatic core -	694	725	707	721
Average ignition delay (ms)	20.2 ± 0.4	-	15.7 ± 0.3	73.5 ± 7
$dP/dt\|_{max}$ (kbar/s)	49.7 ± 4.7	-	20.6 ± 2.6	3.61 ± 1

Table 1: Average values of pressures, temperature, auto-ignition delay and maximum rate of pressure rise for HCCI and SICI combustion. Moderate differences between optical configuration A and B result from a small difference in volumetric compression ratio. Ignition delays are based on maximum rates of pressure rise, with a time origin at TDC. Maximum values of difference with average are also reported. RF discharge triggered 12 ms before TDC in SICI mode.

3.1 Phenomenology of HCCI combustion

3.1.1 HCCI combustion with short ignition delays

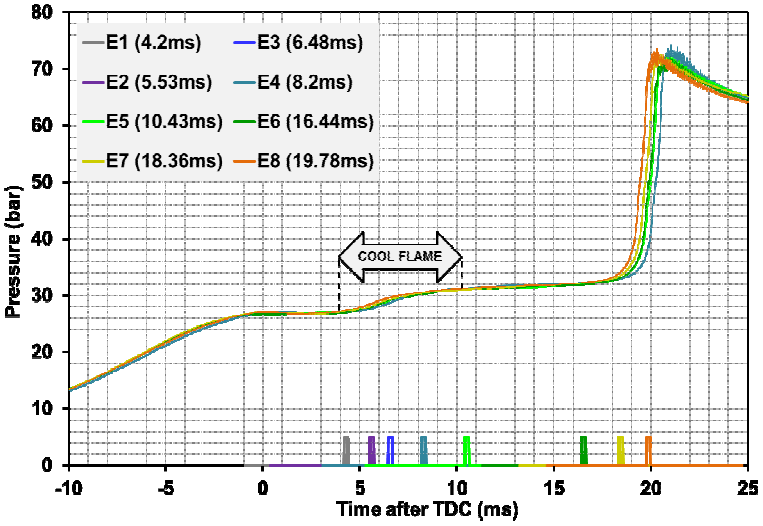

Figure 2: Pressure evolutions and trigger signals of PLIF records during HCCI combustion with short ignition delays. Iso-octane – air mixture at $\Phi = 0.5$, $P_{TDC} = 26.9$ bar, optical configuration A.

Figure 2 displays pressure evolutions obtained during auto-ignition of a lean iso-octane - air mixture (Φ=0.5) at initial temperature $T_0 = 294 \pm 1$ K. An average pressure $P_{TDC} = 26.9$ bar is reached at the end of compression stroke. Eight experiments - reference numbers included between E1 and E8 - are performed in the same conditions, with optical configuration A. For clarity purposes, Fig. 2 displays four of these pressure traces, the first maximum of pressure at t = 0 ms corresponds to the end of compression stroke, e.g. the total volume of the chamber remains constant

from this instant. As a result, pressure is almost the same for three milliseconds. This corresponds in fact to a very slow pressure decrease resulting from heat transfer phenomenon [24]. It is followed by a smooth rise in pressure between 3 and 10 ms, as a consequence of the first stage of heat release, e.g. the cool flame. After that, heat release is considerably reduced resulting in a very slow increase in pressure until the occurrence of the second stage - hot ignition -, at t = 20.2 ms on average, see Tab. 1.

On the same figure are also reported the trigger signals of PLIF imaging: the camera intensification is triggered at the rising edge. As the frequency of the laser is limited to 10 Hz, a single PLIF image is obtained per experiment with optical configuration A. The evolution of PLIF images discussed in the following therefore results from different experiments carried out in identical conditions. A low scatter of pressure traces is observed in Fig.2. Therefore PLIF images in Fig. 3 are arranged in an order representative of the development of combustion: images E2 and E3 are exchanged to account for the late phasing of the cool flame of experiment E3. Other images follow the chronological order.

Figure 3 displays at different instants the simultaneous PLIF and chemiluminescence images. The piston is located at the bottom of the image and the cylinder head is located at the top of the pictures. Each pair of image corresponds to a single experiment. As the fast camera is not equipped with an intensifier, chemiluminescence emission is only visible from the beginning of the second stage of ignition. In the present work, the authors take advantage of this effect to monitor the development of hot ignition zones by chemiluminescence imaging, e.g. this diagnostic is used as a marker of high temperature reactions. The hot ignition period occurs between 18 and 20 ms in these HCCI experiments. As expected, chemiluminescence signal is only detected from these instants. Then, the recorded images display a fast reactive front propagating from the upper corners of the vessel to the whole combustion chamber.

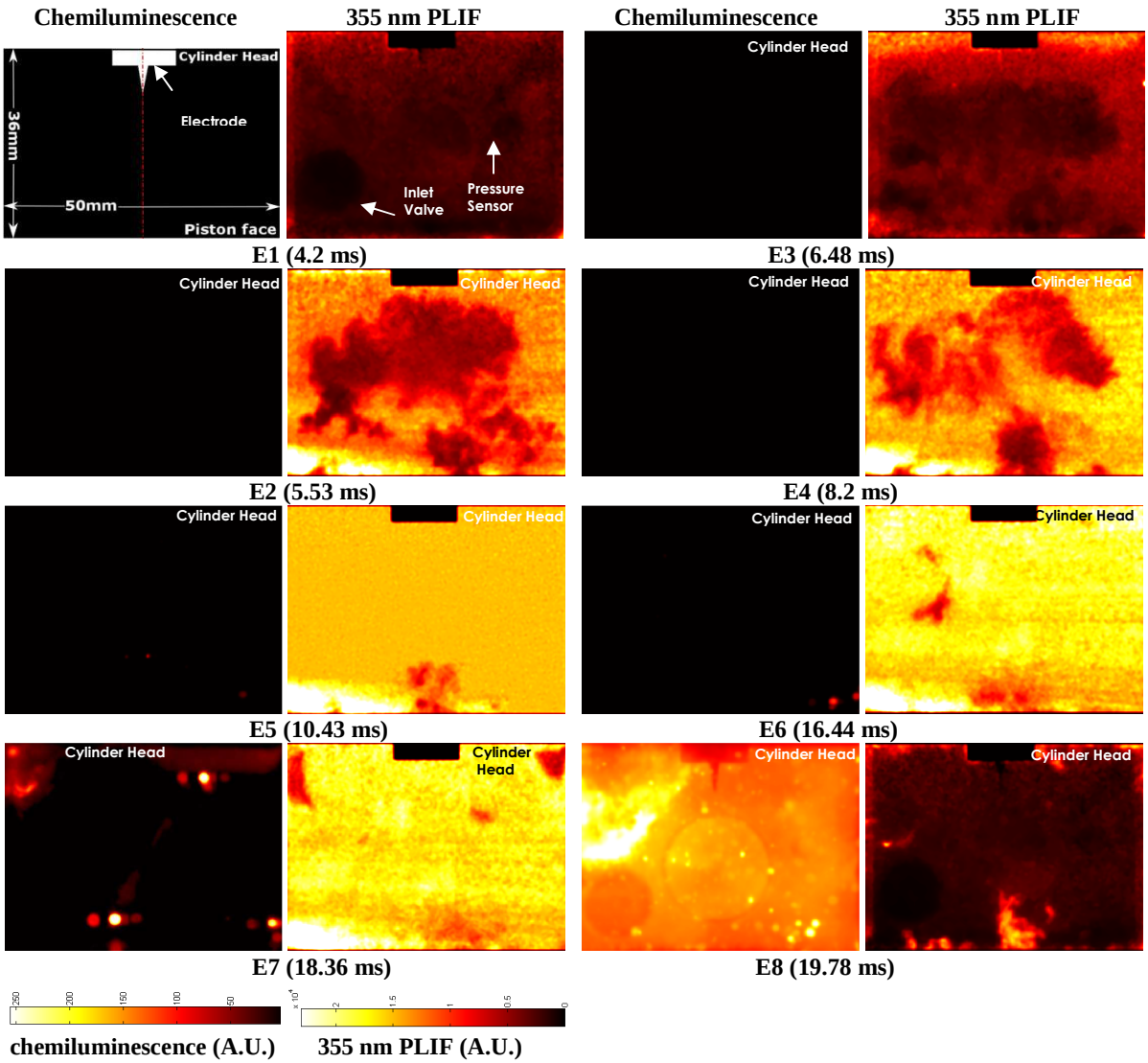

Figure 3**:** Simultaneous chemiluminescence and 355 nm PLIF images recorded during HCCI combustion with short ignition delays. Iso-octane – air mixture at $\Phi = 0.5$, $P_{TDC} = 26.9$ bar, optical configuration A.

Fluorescence images bring additional insights into the understanding of the involved phenomena: intermediate species such as formaldehyde are produced during the cool flame. Intensity of the fluorescence signal progressively increases from t = 4 ms, which corresponds to the beginning of the first pressure rise, as depicted in Figs 2 and 3. It should be noted that in this configuration A, fluorescence records display dark and bright disks at the bottom-left and at the middle-right positions. These contributions from the background are attenuated by the background image subtraction, but they are not fully removed in experiment E1 for instance. They correspond respectively to the inlet valve and the pressure sensor. Heterogeneities depicted in the formaldehyde PLIF images between 5 and 8 ms after TDC are the signature of the thermal stratification within the

chamber at these instants, which is further discussed in paragraph 3.1.2. After these instants, intensity of fluorescence signal also progressively increases at the center of the chamber. Fairly homogeneous fields are thus obtained after the end of the cool flame, between t = 10 ms and t = 16 ms. At t = 18 ms dark zones in the upper corners of the chamber show formaldehyde is consumed, revealing hot ignition is starting. This is consistent with the chemiluminescence image at the same instant, where signal is obtained near the upper corners. This location probably corresponds to a hot core zone: the temperature PLIF measurements of Ben Houidi et al. [11], see Fig. 4, - with an inert mixture and a lower compression ratio - show a small hot zone remains at 18.6 ms in the top corners of the chamber. It is also close to the colder corner vortices, see Fig. 4. Furthermore, it clearly appears in Fig.3 that hot ignition ends in the initially colder gas, which is located near the piston [11,30]. This corresponds to a typical PTC (Positive Temperature Coefficient) behavior of ignition delay, as evoked in [32].

The images corresponding to experiment E8 are obtained at the end of hot ignition at about t = 20 ms. They are qualitatively different from the previous ones: formaldehyde is fully consumed, except near the center of the piston surface. This information cannot be gathered from chemiluminescence as with this line-of-sight integrated diagnostic method, the images display signal issued from the complete visualization zone. This highlights the complementarity of the data provided by the two diagnostic methods.

3.1.2 Focus on the cool flame phenomenon

As previously discussed, Fig. 3 displays a progressive increase in fluorescence level from t = 4 ms, which corresponds to the beginning of the first pressure rise. This result is consistent with intensified chemiluminescence visualizations attributed to CH_2O^* by Griffiths and Whitaker [32] in a similar device. Furthermore, the fluorescence fields are not homogeneous but rather display large scale heterogeneities.

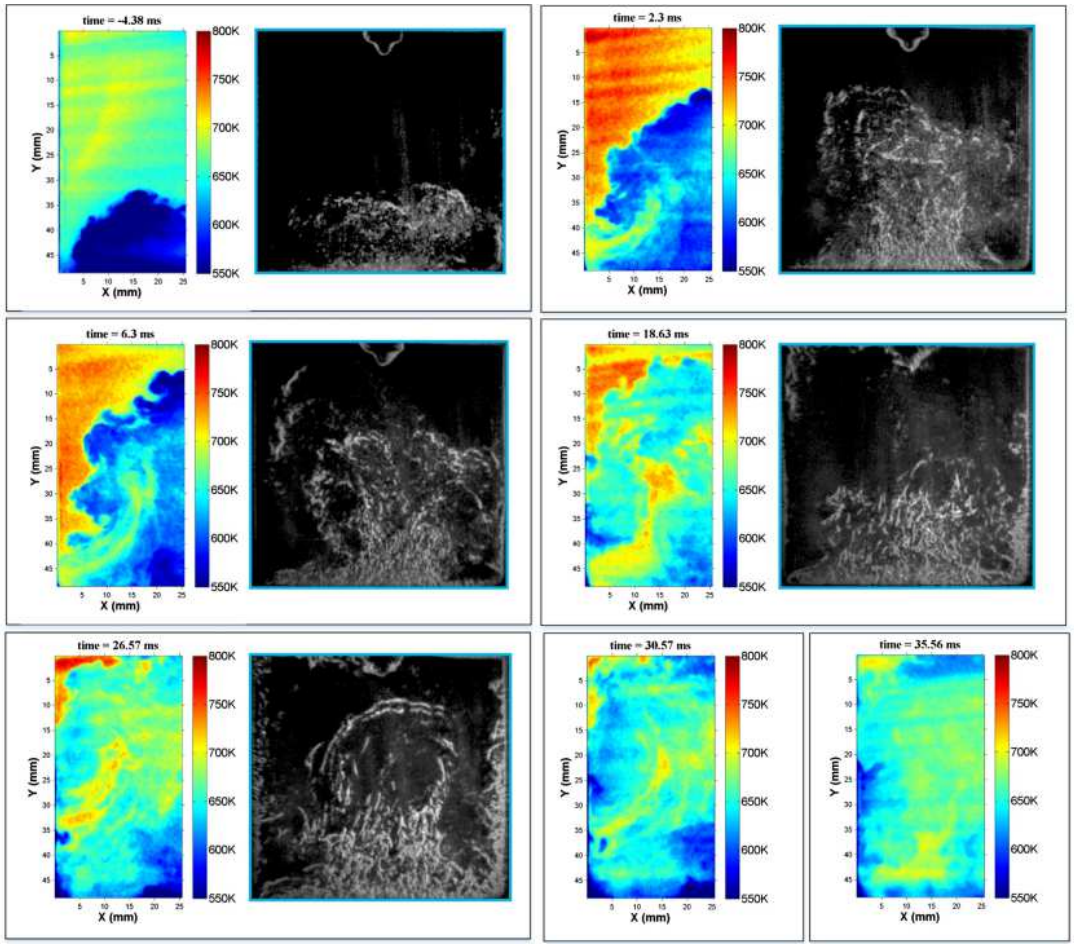

Figure 4: Temperature distribution in the left part of the RCM combustion chamber at different instants during and after the compression of an inert mixture. Quantitative measurements by toluene PLIF are compared to Schlieren images at the same instant. Conditions at TDC: P_{TDC} = 10.7 bar, adiabatic compression temperature T_{ac} = 773 K. Gas composition for Schlieren tests: O_2/N_2/Ar 16.2/6.5/77.3% molar. Volumetric compression ratio: 9. Reprinted from [11] with the permission of Elsevier.

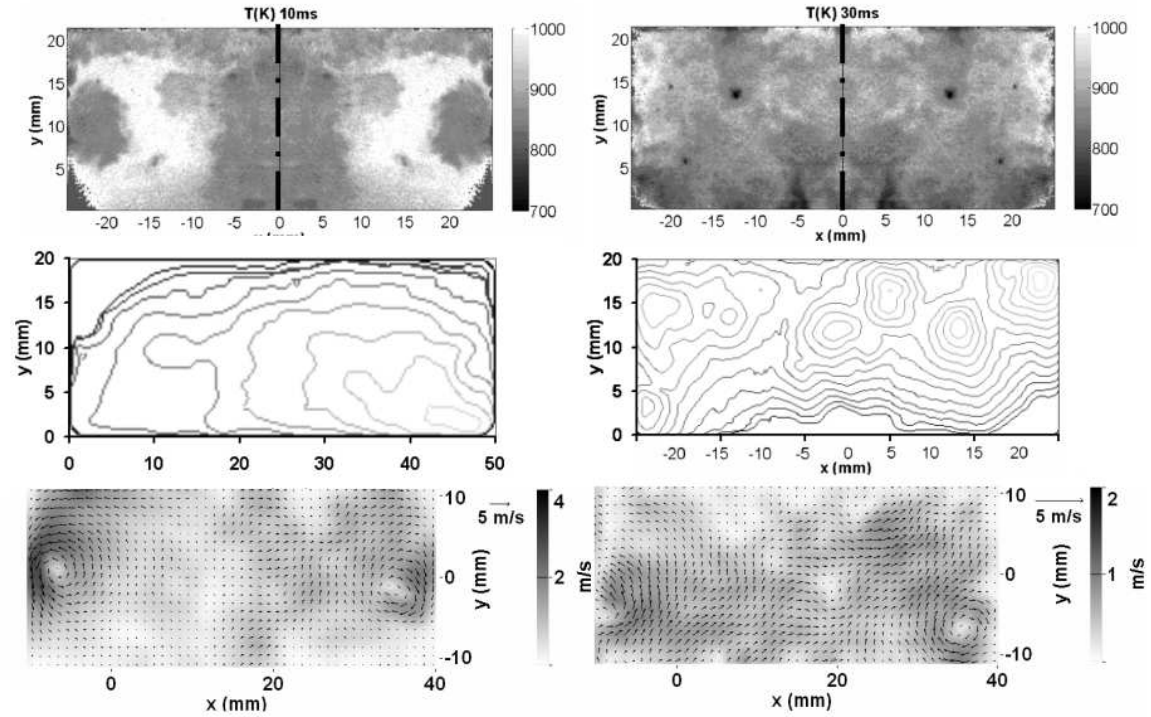

Figure 5: Comparison of the temperature fields (top), direct light emission contours (middle) and velocity fields (bottom) for a volumetric compression ratio equal to 18. The temperature and velocity fields correspond to inert compression experiments at t= 10 ms (left) and 30 ms (right) with pure nitrogen. They are compared to emission contours of reactive compression experiments with CH_4-air mixture featuring ignition delay values respectively equal to 10 ms (left) and 33 ms (right). For more details, see [10].

Two dimensional temperature measurements were performed in the same device by toluene PLIF with excitation at 266 nm, during compression of inert mixtures with different volumetric compression ratio of respectively 9 [11], 12.5 [30] and 18 [9]. Some results are reported in Fig. 4 and Fig. 5. In all these studies, a relatively cold zone delineated by strong gradients was observed at the center of the chamber at TDC. The contours of this cold zone are very similar to that observed in Fig. 3 by formaldehyde PLIF during the cool flame. In the next paragraph, the 355 nm PLIF images obtained in the present work are analyzed at the light of these temperature distributions. They result from the internal aerodynamics, which is typical of flat piston RCMs, see Fig. 5 [10]: the piston moves the cold boundary layer at the center of the chamber during compression, leading to the formation of corner vortices. A hotter zone with low velocities and without fluctuations, called the hot core zone, persists until mixing with colder gases makes it disappear few tens of milliseconds later. This instant is delayed for lower compression ratio values, but the phenomenology described above does not significantly change [31,33]. Magnitude of the velocity is

maximum at TDC in the cold zone and it decreases with time as the corner vortices slowly move downwards and dissipate. Velocity fluctuations are mainly observed in the cool zone and at the frontier between hot and colder region. More quantitative data is provided in §3.2 and the reader is also referred to [10, 30, 31, 33] for more details.

On the one hand, ignition delays of the cool flame are known to decrease with rising temperatures for such hydrocarbons. On the other hand, Fig. 3 shows the 355 nm fluorescence signal recorded at these instant is intense in the lateral regions surrounding the central zone, where the fluorescence level is weak: the former corresponds to the hottest region, the latter to a colder one in Fig. 4. The temperature dependence of cool flame phenomenon is at the origin of this observation: the low level of progress of cool flame reactions at this colder location results in a lack of fluorescent species observed in Fig. 3 in this region at about 5 ms after TDC.

This observation is consistent with the analysis reported in [32] for a flat piston rapid compression machine using chemiluminescence. Nevertheless, the present results provide more information, as the direction of the observation is here perpendicular to the cylinder axis: from -5 ms to TDC, the hot and colder regions are more clearly put into evidence in the measurement plane by 355 nm PLIF, but also by line of sight integrated methods like schlieren, see Fig. 4. In particular, the absence of density gradients in schlieren images at the top of the chamber, e.g. in the hot region at these instants, confirms the observations made in the vertical plane by 355 nm PLIF are representative of the whole chamber in terms of temperature distribution: the cold zone is surrounded by a hotter region, where the cool flame appears first.

In conclusion, these experimental results prove that heterogeneities depicted in the formaldehyde PLIF images are the signature of the thermal stratification within the chamber at these instants.

Additional results are reported in Fig. 6. Fluorescence images are obtained with the double pulse 355 nm imaging system, e.g. with optical configuration B: the four lateral walls are fitted with windows, which also enables a more homogeneous background image and thus a better visualization of the cool flame phenomenon. Temporal evolution of the latter can be followed using

the double pulse PLIF feature of configuration B. Identical mixture and fairly close experimental conditions are considered here, see Tab. 1. Nevertheless, a slightly higher temperature is reached at TDC in configuration B, therefore the cool flame in that case occurs earlier than in configuration A.

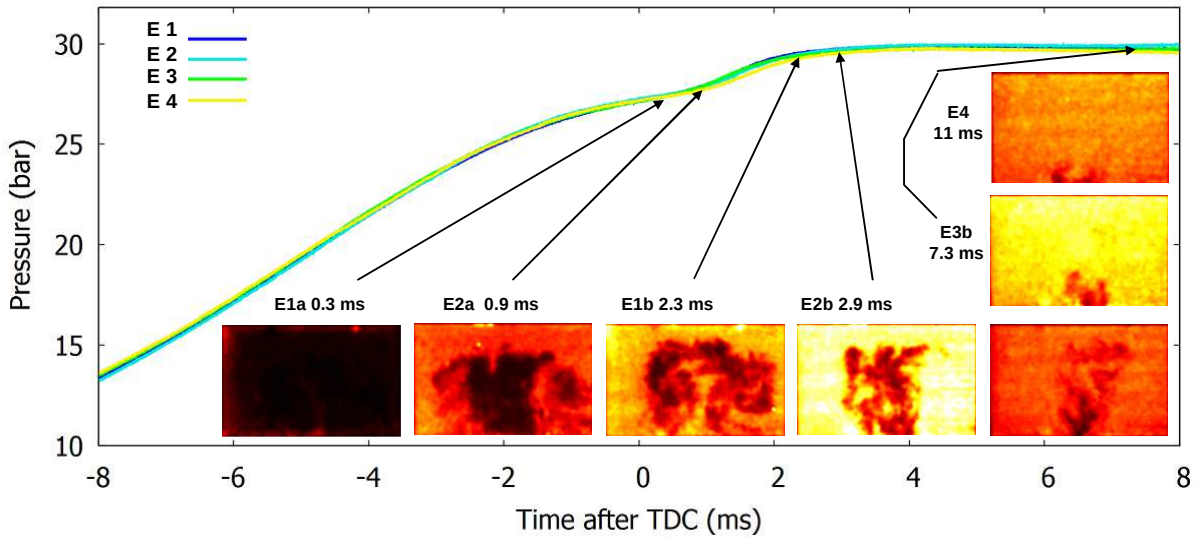

Figure 6: Pressure evolution and 355 nm fluorescence images during cool flame period.
Optical configuration B. P_{TDC} = 27.4 bar.

Figure 6 reports the fluorescence images obtained during the cool flame period for different experiments and different instants. Corresponding pressure traces are also included. These images confirm the phenomenological analysis obtained above from Fig. 3: the increase in fluorescence levels is clearly evidenced near the top and lateral walls, e.g. in the hot region. Then the dark zone seems to shrink, which is clearly evidenced during a single experiment, see images E2a and E2b. In particular, high levels of fluorescence appear in the corner vortices near the lateral walls and then progressively spread across the central zone. At last, the signal level increases near the bottom-center of image e.g. near the piston and a homogeneous field is recorded 11 ms after TDC.

It is recalled the dark zone observed at 0.9 ms is relatively cold before any heat release from the cool flame, see Fig. 4. Such a thermal stratification is induced by internal aerodynamics, which is typical of flat piston RCMs. This confirms the positive temperature dependence of cool flame ignition delay is at the origin of the observed ‘shrinking’ of the dark zone: fluorescent species produced by the cool flame appear sequentially, as the cool flame occurs first in the hottest regions and then progressively in initially colder regions. In other words, the cool flame propagates in the

cold region. To the authors knowledge, this phenomenon is observed for the first time during the auto-ignition of premixed fuel-air medium in a RCM. Cool flame propagation was also recently observed during strong auto-ignition in constant volume chambers [35]. One may remark it is also observed during the auto-ignition of diesel sprays, see for instance [36,37].

Furthermore, the shape of the dark zone is still wrinkled close to the end of the cool flame process, see for instance E3a and E3b in Fig. 6. This highlights the presence of temperature heterogeneities observed in Fig. 4 not only at the frontier between the cold and hot region, but also in the core of the initially colder zone. Finally, the two pairs of images reported in Fig. 7 evidence significant cyclic fluctuations of the frontier between the hot and colder zone, as mentioned in [10] with the same device but with a higher volumetric compression ratio. The presence of temperature heterogeneities in the colder zone is also revealed by fluorescence images E5b and E6b.

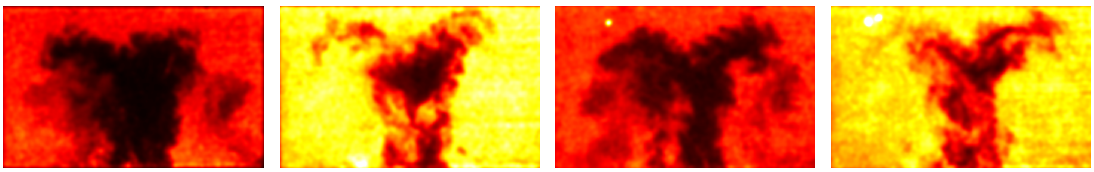

E5a 1.8 ms **E5b 3.8 ms** **E6a 1.8 ms** **E6b 3.8 ms**

Figure 7: PLIF Images obtained during HCCI combustion, short ignition delays, P_{TDC} = 27.4 bar, optical configuration B. Each pair of images is recorded during a single experiment

3.1.4 HCCI combustion with long ignition delays

Additional HCCI experiments are performed with optical configuration B at lower pressure values P_{TDC} = 19.6 bar, see Tab. 1. Ignition delays are increased at this lower pressure value. The effect of this parameter is investigated here as previous studies with the same RCM [10,11] evidence ignition delay strongly affects the HCCI combustion process. In particular the local mode of combustion (autoignition versus deflagration) and thus the global heat release rate are strongly dependent on the ignition delay value.

In this section, the same reactive mixture as previously is considered with optical configuration B, e.g. with the double pulse PLIF system. Figure 8 displays the recorded pressure traces. Trigger signals are surimposed and fluorescence fields are still recorded at the positive edges. Several pairs of images are recorded, each of them represent a single compression experiment (E1a E1b and E4a,

E4b). Pressure evolutions are highly reproducible, except during hot ignition, as a relatively low scatter of ignition delay is observed: maximum value of the difference with average are close to 10 % of the mean ignition delay value, see Tab. 1. A value of about 6 % is reported in [33] for similar conditions. Low cyclic fluctuations levels are also reported for short ignition delays: lower than 2 % here, and 8 % in [33]. The origin of these fluctuations is further discussed at the end of the section. As expected [10], much lower rates of pressure rise are obtained for these large ignition delay values in comparison to the other HCCI results with short ignition delay, see Tab. 1.

The combined chemiluminescence and PLIF images are reported in Fig. 9. They present similarities with the higher pressure case: no chemiluminescence signal is recorded for a long period after TDC, see Fig. 9 at 2.86 ms up to 31.22 ms. In fact, chemiluminescence is detected only during the hot ignition stage, which often starts with a multi-site combustion, as shown in this figure at 64.68 ms. No preferential location of the first kernels is found, as reported in [10]. It is worth noticing a slower front propagation from each hot ignition kernel follows, see § 4.4 for a quantitative analysis. Similar observations were reported for relatively large ignition delays in [10,24], which is summarized as follow: at late instants there is enough time for the hot core to be subjected to mixing, but thermal stratification is not completely removed and small hot zones remain within the chamber, leading to multi-site ignition [9,10,30]. 355 nm PLIF images are similar to that of previous Fig. 3. A homogeneous fluorescence field is obtained as late as 64.68 ms after TDC, and hot ignition is detected by chemiluminescence from about t = 59 ms, e.g. out of the PLIF measurement plane for this experiment E3. A dark zone corresponding to hot ignition is detected a few milliseconds later in the PLIF images. Indeed, experiment E4 features two successive fluorescence images recorded during an intermediate stage of hot ignition, at t = 65.59 and 67.59 ms. The reactive front displays a wrinkled shape, with relatively low propagation velocities representative of a deflagration, which is further discussed in paragraph 4.4. Similar fluorescence images are reported in [25] with configuration A, but with multiple kernels. All these results suggest a transition in combustion regime occurs for these long ignition delays, changing from auto-ignition to deflagration. This would be consistent with the reduction of the maximum rates of

pressure rise reported for these higher values of ignition delay. As evoked above, such a transition to deflagration is related to the fairly high gradient values delineating the small hot zones remaining in the vessel at late instants, e.g. corresponding to these large values of ignition delay [10,30]. The phenomenon observed in our previous work for methane–air mixtures is confirmed here for a heavier hydrocarbon in the presence of two-stage ignition.

It can be noticed chemiluminescence records evidence a larger combustion zone than in fluorescence images. A second combustion kernel is also observed. This illustrates again the difference between the planar and line-of-sight integrated diagnostic methods, and underlines the complementarity of both approaches when used simultaneously.

Combustion stability is a key issue of HCCI combustion and closed loop control is a possible way to reduce cycle-to-cycle variability of HCCI engines [38,39,40]. As stated above, relatively low cycle-to-cycle fluctuations of combustion phasing are obtained with the present RCM. The authors propose a new and original analysis of the relatively low scatter of ignition delay in the HCCI case, as obtained in the present device. For short ignition delay, the low scatter of ignition delay (< 2 % here, 8 % in [33]) results from aerodynamics which is typical from flat piston RCM with initially quiescent mixtures: as long as the homogeneous hot core zone exists, see Fig. 4 and 5, the adiabatic core hypothesis holds. Temperature follows a highly reproducible history imposed by quasi-identical pressure evolutions before hot ignition, see Fig. 6. That is why even if the frontier of this zone varies between consecutive experiments, see. Fig. 7, auto-ignition occurs at close instants for short ignition delays. The case of long ignition delays is less straightforward: adiabatic core assumption may finally be invalidated [8], as the hottest gas region is partially mixed with colder gas for sufficiently long delays [9,11]. Fluctuations of the frontier of the hot zone observed at earlier instants in Fig 7, as a result of turbulence, may *a priori* affect the maximum temperature values in the chamber when the frontier disappear. This could lead to an increase in fluctuations of ignition delays. In practice, such a behavior is not observed for long ignition delays as in this case maximum differences in ignition delays remain lower than 10%, see Tab. 1 - and less than 6% in similar conditions in [33].

Furthermore, if cycle-to-cycle variability seems to be moderate, the temperature distribution for short ignition delays, e.g. a large homogeneous hot zone, is specific to flat piston RCM aerodynamics and probably is fairly different from that of an HCCI engine. Nevertheless, for long ignition delays, this homogeneous zone disappears, and the heterogeneous temperature distribution resulting from the turbulent and structured flow is probably more representative at these instants of the temperature distribution observed in engines. For these reasons, the phenomenological analysis reported herein in the flat piston RCM for long ignition delays can be relevant to the HCCI combustion processes as they occur in engines.

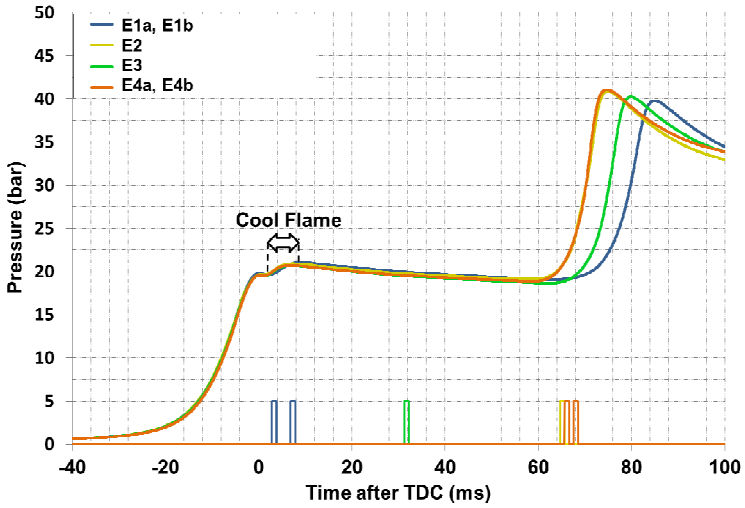

Figure 8: Pressure evolutions and trigger signals of PLIF records during HCCI combustion with long ignition delays. Iso-octane – air mixture at Φ = 0.5, P_{TDC}=19.6 bar, optical configuration B.

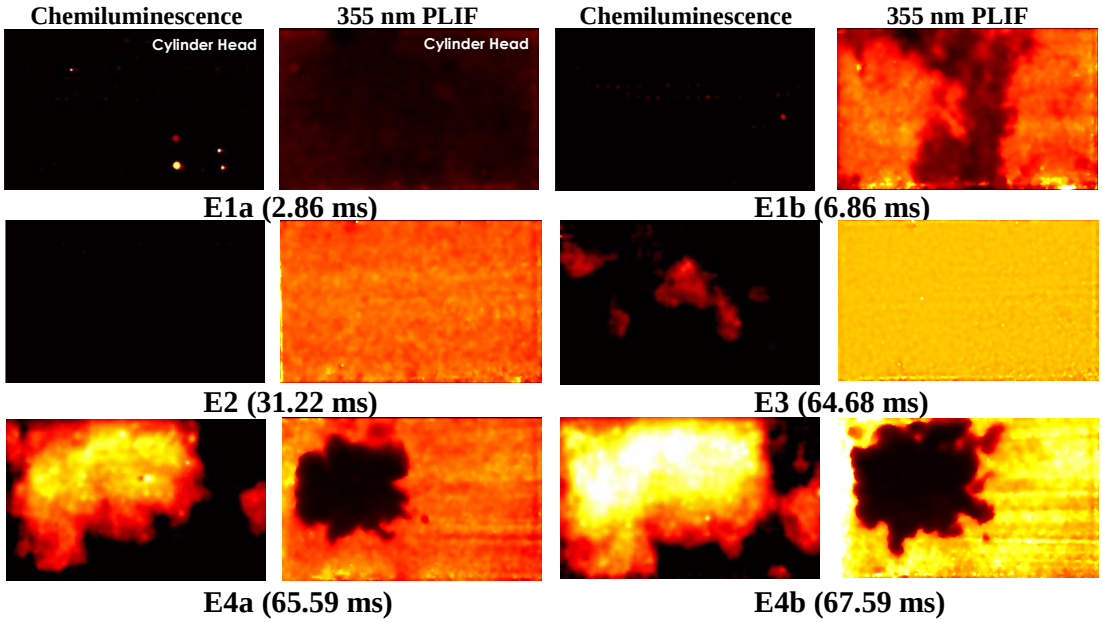

Figure 9: Simultaneous chemiluminescence and 355 nm PLIF images recorded during HCCI combustion with long ignition delays. Iso-octane – air mixture at Φ = 0.5, P_{TDC} = 19.6 bar, optical configuration B.

3.2 Phenomenology of SICI combustion

Spark Induced Compression Ignition (SICI) experiments are performed with optical configuration A. The same reactive mixture is employed in the same conditions as the previous autoignition experiments - see Tab. 1 - except two points: (i) Chemiluminescence images are recorded by a Princeton PIMAX intensified camera with a low level of intensification and a 100 μs gate value. The higher sensitivity of the camera enables the detection of the flame while the level of the light emission is very low. Furthermore, (ii) ignition is triggered 12 ms before the end of compression, see Fig 10. A radiofrequency (RF) discharge [41] is employed for this purpose and 305 mJ of electrical energy is provided to the electrode in one millisecond. These characteristics were found ideal to observe a SICI effect with this lean isooctane-air mixture, see §2.1 and [25]. It is worth noting the equivalence ratio of the gaseous mixture $\Phi = 0.5$ equals the lower flammability limit (LFL) at ambient conditions – 0.8 % in volume at 24°C - [42], which means a flame would not propagate in this mixture at atmospheric pressure and ambient temperature with a low energy igniter. In the present case, the combination of the high amount of energy provided by RF discharge and the compression effect - leading to high pressure and temperature conditions - make possible the flame propagation within the combustion chamber. This is confirmed by Martz et al. [45] who performed 1D computation of flames propagating in isooctane-air mixture at 1000 K and 20 bar, but for an initially homogeneous temperature field: propagation in deflagration regime is mostly observed, while lower contribution of heat conduction, e.g. auto-ignition front, was only observed shortly before bulk auto-ignition. At these instants, the front only propagates over a distance representative of the flame thickness as all the remaining unburned mixture auto-ignites. At the final stage of the combustion process, the pressure rise is steeper as the end gas autoignites at 15.7 ms on average. This value is slightly lower but similar to that of the short ignition delay case in HCCI mode, see Tab. 1. It is worth noticing for similar TDC conditions, the maximum rate of pressure rise remains lower in the SICI case than in HCCI mode, with respectively 20.6 kbar/s instead of 49.7 kbar/s. A similar conclusion can be drawn for the time average of the rate of pressure rise. This smoother heat release process illustrates the relevance of SICI combustion mode

for practical applications in engines.

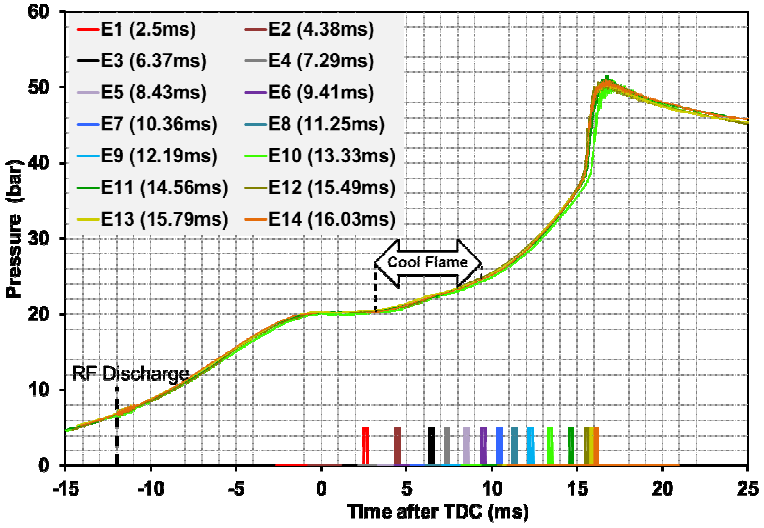

Figure 10: Pressure evolutions and trigger signals of PLIF records during SICI combustion.

Discharge is triggered at -12 ms. Iso-octane – air mixture at $\Phi = 0.5$, $P_{TDC} = 20.3$ bar. Optical configuration A.

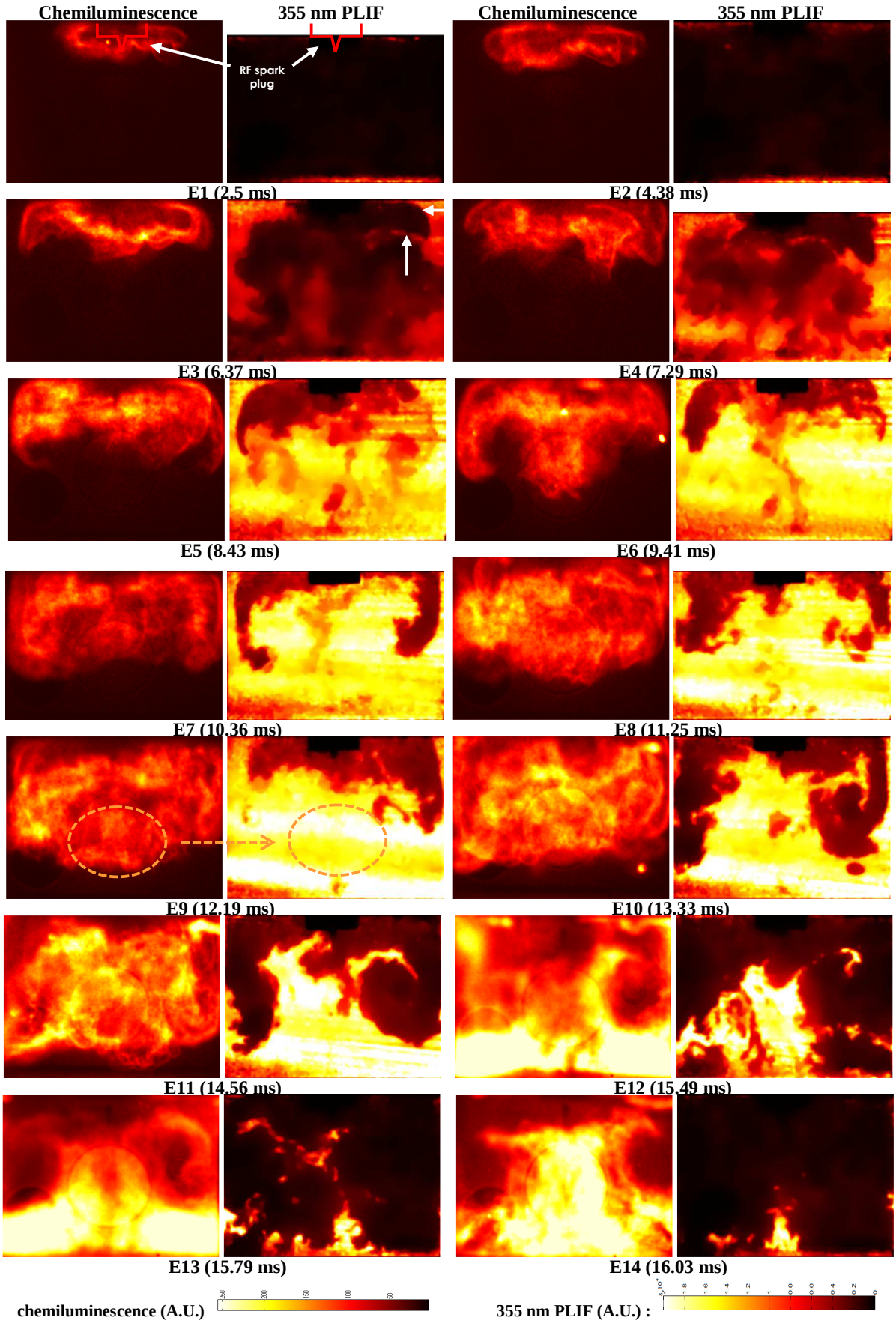

Figure 11: Simultaneous chemiluminescence and formaldehyde PLIF images recorded during SICI combustion. Discharge is triggered at -12 ms. Iso-octane – air mixture at Φ = 0.5, P_{TDC} = 20.3 bar, Optical configuration A.

RF spark plug is reported in red solid line. Orange dashed lines highlight the difference between planar and line-of-sight integrated measurements. White arrows show the position of the flame for experiment E3.

Pressure evolutions are reported in Fig. 10. The corresponding chemiluminescence and PLIF images are depicted in Fig. 11. The fluorescence images reported in Fig. 11 include background and laser sheet homogeneity correction. Discharge ignition occurs at t = -12 ms. It is followed by the end of compression at t = 0 ms. A slow flame propagation is observed by chemiluminescence near the cylinder head during this period. The cool flame then occurs between 2.5 and 7.5 ms, but fluorescence signal appears more clearly from 6.3 ms (E3). It is located near the lateral walls of the chamber and displays the wrinkled contours of the colder zone, as described in the previous HCCI case §3.1.2. A slightly darker zone is also observed near the cylinder head, see the white arrows in E3, Fig. 11. Delineated by smooth contours, it corresponds to the flame initiated earlier by the RF igniter, as fluorescing species were consumed by the flame in the burned gases. This suggests the upper part of the premixed flame remains laminar at this instant. This is consistent with the low velocities measured with the same device for the same compression ratio: average velocity is lower than 0.7 m/s at the igniter location at TDC, e.g. close to these instants [30]. Furthermore, a lower level of velocity fluctuations was reported in this zone [34]. The PLIF images shown here at 6.3 ms suggest the lower part of the flame is probably affected by the upper part of the corner vortices. This is consistent with [30] as velocities in these structures vary between 0.7 and 2.5 m/s in inert case (10 ms after TDC, for P = 20 bar at TDC).

From t = 8.4 ms (E5), fluorescence signal is observed in the whole investigation zone except in the mixture burned by the flame. At these instants, PLIF images appear as the ‘negative’ of chemiluminescence images. The authors underline that the flame does not propagate within fully unburned mixture since PLIF images show the presence of intermediate species like formaldehyde ahead of the flame front. Instead, the flame consumes the products of cool flame, e.g. the flame propagates within a pre-reacted gaseous mixture. This probably affects the flame velocity. Indeed, in the framework of MILD combustion, Sidey et al. [46] reported that the presence of minor species - like formaldehyde - affects the flame velocity of methane and air premixed with burned gases at high dilution ratio, e.g. at high temperatures. In particular, an increase in flame velocity was

reported in the presence of minor species as the premixed flame was getting closer to an auto-ignition problem. This is relevant to the SICI process under study here, during and after the cool flame process. An acceleration of the flame was also reported by Martz et al. [45] shortly before the auto-ignition instant, in the case of a hot and lean mixture of iso-octane and air.

Fluorescence images obtained at 9.41 ms (E6) and later clearly evidence the motion of the flame front induced near the lateral walls by the corner vortices: the fluid flow tends to increase flame surface at these instants. Furthermore, it is worth noticing the shape of this front becomes progressively wrinkled, which is clearly displayed in Fig. 11 from t = 11.25 ms (E8). This suggests a significant influence of both average velocity and velocity fluctuations on the flame propagation at these instants. From a quantitative point of view, a maximum value of velocity fluctuations of 0.5 m/s was measured in the cool zone in the same device, at the center of the chamber 2 ms before TDC but with higher compression ratio [10,33]. Lower apparent velocities of S_a = 0.35 m/s – burning velocity relative to the burned gases - , and consequently lower burning velocities relative to the unburned mixture, are estimated in §4.2 in the present SICI condition between -5 and 2 ms after TDC. This confirms the wrinkled front observed in Fig. at t = 11.25 ms and later is the signature of turbulence affecting the flame shape.

By contrast, chemiluminescence images recorded at 10.36 ms and later display a flame front with a smooth shape propagating vertically towards the piston. This results from the three dimensional shape of the flame front: light is integrated along the optical path in chemiluminescence records and the PLIF images show the flame is convected by the corner vortices – with velocities higher than the burning velocity Sa evoked above -. These vortices feature an approximately toroidal shape: that is the reason why chemiluminescence emission is detected at the center of the chamber while the fluorescence intensity is still high at the same location, see the dashed lines at 12.19 ms: the flame did not reach the center of the chamber – close to the cylinder axis - at this instant. Moreover, the combined PLIF 355 nm and chemiluminescence diagnostics put into evidence the interaction of three phenomena: (i) the flame consumes a pre-reacted gaseous mixture, (ii) the flame front is affected by the large-scale post-compression aerodynamics and in particular by corner vortices, and

(iii) it becomes progressively wrinkled by small scale vortices attributed to turbulence. Such phenomena are expected to influence the flame propagation velocity, and consequently the heat release rate, which affects in turn the autoignition process.

A sharp increase in pressure occurs approximately between t = 15.5 and 17 ms, corresponding to the second stage of auto-ignition process, e.g. hot ignition. At these instants, chemiluminescence emission is observed over the full field of investigation. Higher emission levels evidence an intense burning zone near the piston. In fact, this phenomenon corresponds to a fast propagation of reactions fronts, which is further discussed in the next section. PLIF images recorded between 15.49 and 16.03 ms bring additional information: the observed phenomena are identified as the successive auto-ignition of gaseous mixture that remained incompletely reacted near the piston corners and later near the center of the chamber. The last PLIF image obtained at t= 16.03 ms shows almost all the formaldehyde is consumed by hot ignition. This is consistent with the pressure signal: for this experiment E14, the instant corresponds effectively to the end of the pressure rise, e.g. to the end of heat release. The irregular shape of the contours of the fluorescence zone can be underlined, which could be the signature of small scale temperature stratification.

One may suggest the flame is laminar at the onset of the combustion process, which does not occur in SICI engines. However, except during this very short period of time, combustion process is more representative of SICI engines as a turbulent flame propagates and it is strongly affected by large structures. The latter decay with time, in terms of size and energy [34]. Furthermore, the assisted auto-ignition process seems to be affected by small scale temperature heterogeneities, as reported for instance by Schließl and Maas in SI engines [47]. To the author's knowledge, the above analysis of SICI combustion obtained in a RCM is reported for the first time.

In order to further analyze the fast dynamics of autoignition, two additional experiments are reported. The first one corresponds to the same mixture and experimental conditions as that presented above in Fig. 11. Configuration A is still used, but a fast camera records chemiluminescence at 40000 fps, see Fig. 12. The focus is on the auto-ignition stage of this SICI experiment, therefore chemiluminescence is observed in the whole field of view at these instants in

Fig. 12. If the intense chemiluminescence zones may appear as instantaneous bulk combustion in previous Fig.11, Fig.12 evidences a fast propagation of more intense chemiluminescence zones, see the black arrows. The motion starts at $t = t_0$ from the top of the chamber near the lateral windows and ends downwards with large zones located near the piston corners. Chemiluminescence images suggest very high apparent velocity values: between t_0+25 and t_0+75 µs, the lowest part of the bright zone is found to propagate downwards at about S_a = 200 m/s, a magnitude order which remains representative of subsonic auto-ignition fronts in the unburned mixture. The binarization algorithm further described in §4.1 is used to detect the contour. However, only the half lower part of the contour is considered here to obtain an estimate of the velocity value. Higher threshold levels are needed at these instants as light collection is line-of-sight integrated and light emission is already detected in the whole field of view at t_0.

Computing apparent velocity values is crucial as they provide information relevant to the nature of the propagation front. As the chemiluminescence diagnostic is line-of-sight integrated, the shape of the combustion fronts is less complex at the onset of the combustion process, and more accurate velocity values can be obtained at these instants. This is the subject of further investigations in the next section §4.

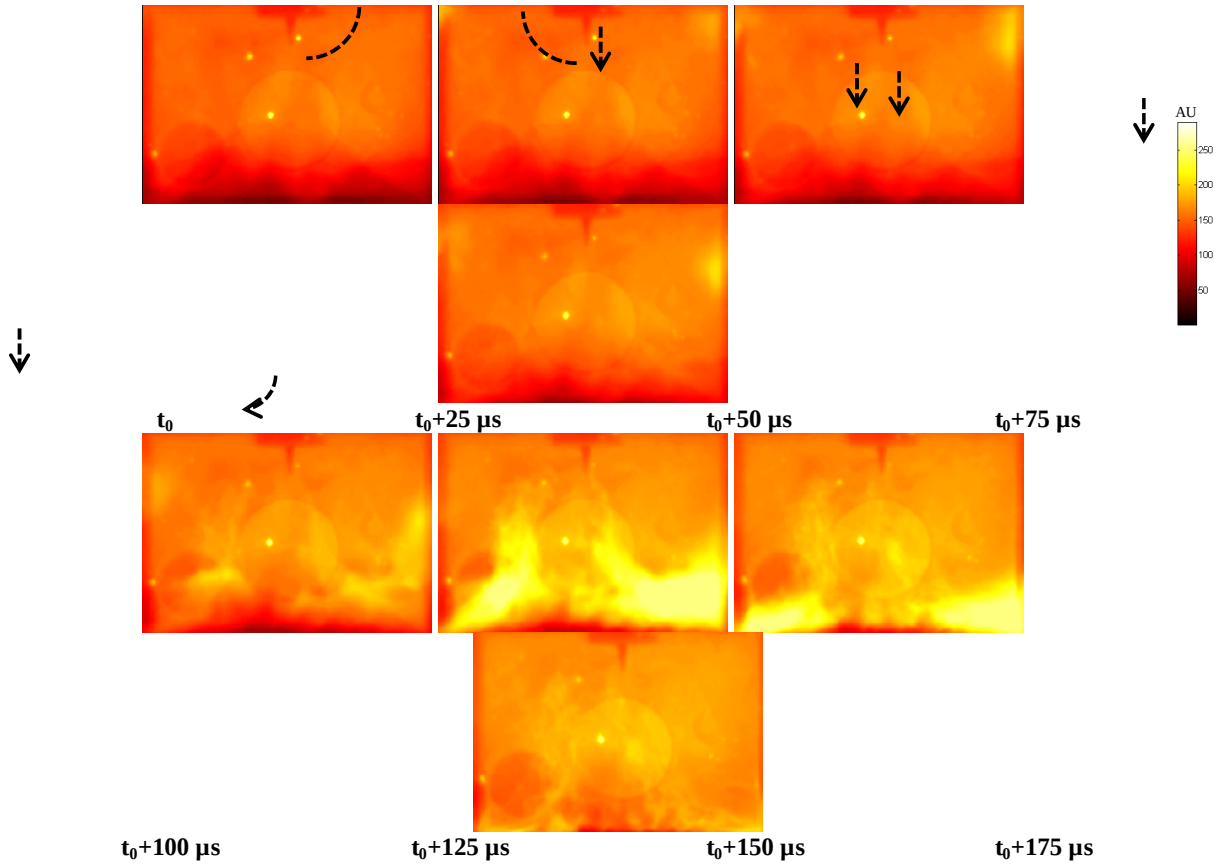

Figure 12: Chemiluminescence recorded at 40 kHz during the auto-ignition stage of SICI combustion. Discharge is triggered at -12 ms. Iso-octane – air mixture at $\Phi = 0.5$, $P_{TDC} = 20.3$ bar. Optical configuration A

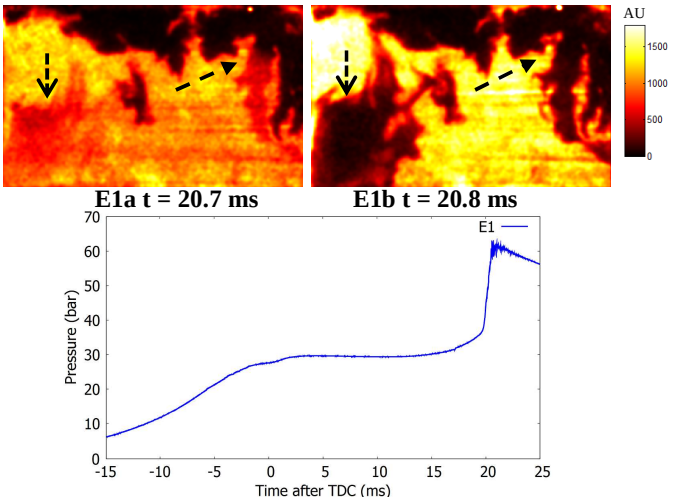

Figure 13: 355 nm fluorescence images (top) and pressure trace (bottom) for a single 'SICI' experiment ignited by incandescent particle at about 10 ms. Iso-octane – air mixture at $\Phi = 0.5$, $P_{TDC} = 27.4$ bar. Optical configuration B.

The second additional experiment is reported in figure 13 in order to investigate the combustion process at these late instants. It displays two successive PLIF images obtained during the same auto-ignition event recorded in optical configuration B, in the high pressure HCCI conditions of Tab. 1. However in that case, deflagration is triggered by an undesired incandescent particle about

10 ms after TDC. The dark zone at the top of image E1a probably results from deflagration, as the analysis of chemiluminescence images show a deflagration propagates in this zone from 12 ms after TDC. At 20.7 and 20.8 ms chemiluminescence emission is observed in the whole visualization zone. Therefore experiment E1 of Fig.13 presents qualitative similarities with the SICI case above, but with a later phasing of ignition. This is confirmed by the pressure trace reported in Fig. 13.

It is worth noticing the left bottom part of image E1b features dark zone which is already present 100 µs earlier in light grey in image E1a, with the same contours – see the left arrow -: the characteristic time scale of the consumption of the fluorescent species is greater than 100 µs. By considering an equivalent spherical propagation centered on this zone, this fast consumption of fluorescent species would lead to an apparent velocity of about 80 m/s, a magnitude order which would be consistent with the high velocities reported above from Fig. 12. This zone may correspond to the hot zone observed under the cold corner vortex in a central measurement plane at the same instant for high compression ratio values [9]. Such a zone also exists for low compression ratio values, but it is smaller at 18.63 ms, see Fig. 4. Furthermore, the high velocity value is consistent with the fast auto-ignition fronts observed in the hot core zone in previous studies in HCCI mode [10]. Nevertheless, the left part of these two images, see the left arrow, rather suggest bulk auto-ignition occurs, rather than a fast propagating spontaneous reaction wave as observed in Fig. 13, or in Ben Houidi et al. [11] for instance in HCCI case. A similar behavior is reported at the right part of the images, but the vertical light grey zone seems to display a vertical gradient in fluorescence level in image E1a, as shown by the right arrow. This suggests there is a transition from deflagration regime to a more volumetric auto-ignition regime. Besides, moderate pressure oscillations are observed at these instants. The existence of bulk – or volumetric - combustion regimes was reported for instance in [43]. In that case it is called inertially confined or nearly constant volume: this mode occurs when the excitation time is shorter than the acoustic time characteristic of the auto-igniting hot spot. The excitation time, which characterizes the main heat release, is observed here through the consumption of the fluorescent species: if the PLIF images in Fig. 13 evidence a relatively short value for the excitation time, the velocity of the front estimated at

80 m/s here remains lower than the speed of sound. As the combustion occurs in a volumetric way, this analysis suggests the expansion of the hot kernel has enough time to occur during auto-ignition. In other words, inertially confined regime does not occur here. It is difficult to draw general conclusions from this single experiment, and more data should be gathered in future studies. Nevertheless, both Fig.12 and Fig. 13 show very different modes of auto-ignition may occur in SICI operating mode, eg. deflagration, spontaneous ignition fronts and a more volumetric – but subsonic - auto-ignition mode.

From a more general point of view, we would like to underline auto-ignition front velocity strongly depends on thermal gradients [10]. Therefore, the latter drives the occurrence of these regimes and their transitions: the results reported here suggest thermal gradients represent a mean to control the different modes of auto-ignition and thus the heat release rate at the end of the SICI process. This contrasts with the chemical composition, pressure and temperature parameters which may affect all the different stages of SICI process.

4. Quantitative analysis of apparent flame velocities

The existence of different propagation regimes was predicted by the early work of Zel'Dovich [44] for fuel-air mixtures at high temperature featuring heterogeneities. Depending on the level of local stratification in temperature or chemical composition, deflagration, auto-ignition or detonation may occur. A significant part of the following research efforts were focused on the delineation of the limits between the different regimes and the associated influent parameters. For more details, see for instance [10,14,15]. The present section focuses on the limit between deflagration and spontaneous auto-ignition fronts, the latter being characterized by higher propagation velocities. In particular, the following work aims at discriminating the propagation regime through the estimations of an apparent velocity of the reaction zones. Cycle resolved data obtained by chemiluminescence are employed to this purpose. It is analyzed at the light of the simultaneous PLIF/chemiluminescence results reported above. Both the SICI and HCCI operating modes of combustion are investigated.

4.1 Methodology

Chemiluminescence emission records are post-processed to compute apparent flame velocity values. Chemiluminescence contours are detected by using anisotropic filters [48] followed by the binarization algorithm documented by Otzu [49]: the threshold level is obtained for each image from its intensity histogram. An apparent velocity is calculated considering the average distance between two consecutive contours divided by the appropriate time step. It is obtained from a centered finite differencing scheme with second order accuracy, see Eq. 1.

$$S_a = 2\frac{A_{n+1}-A_{n-1}}{(L_{n+1}+L_{n-1})(t_{n+1}-t_{n-1})} \quad (1)$$

Where A_n is the area inside the contour and L_n is the contour length at the time step t_n. This relation represents an average of the apparent flame velocity, e.g. in the frame of reference of the laboratory. It is a good approximation provided that (i) reasonably short time steps are employed, (ii) these time steps lead to a sufficient motion of the front, e.g. a sufficient number of pixels. Therefore chemiluminescence records are sub-sampled at low velocity values.

The post-processing is employed close to the onset of light emission from hot ignition. Indeed, reaction zones observed near the end of the combustion process feature more complex shapes, where 3D effects make quantitative analysis more difficult with a line of sight integrated method.

4.2 Propagation of reactive fronts: SICI experiments

Configuration A is employed but the beamsplitter was removed for these experiments to improve light collection. The corresponding contours of chemiluminescence emission are reported in Fig. 14-a at several instants. Different colors are employed as a function of time: contours at earliest instants are reported in red and then progressively change to blue with time. For both readability and accuracy purposes, data are subsampled and two consecutive contours are separated by 0.5 ms in Fig. 14-a. Contours depict the flame propagation within the chamber. From a phenomenological

point of view, the results are similar to visualizations reported in Fig. 12. As the focus is on the beginning of the combustion process, the second stage of auto-ignition at the end of the SICI process is not quantified here by chemiluminescence.

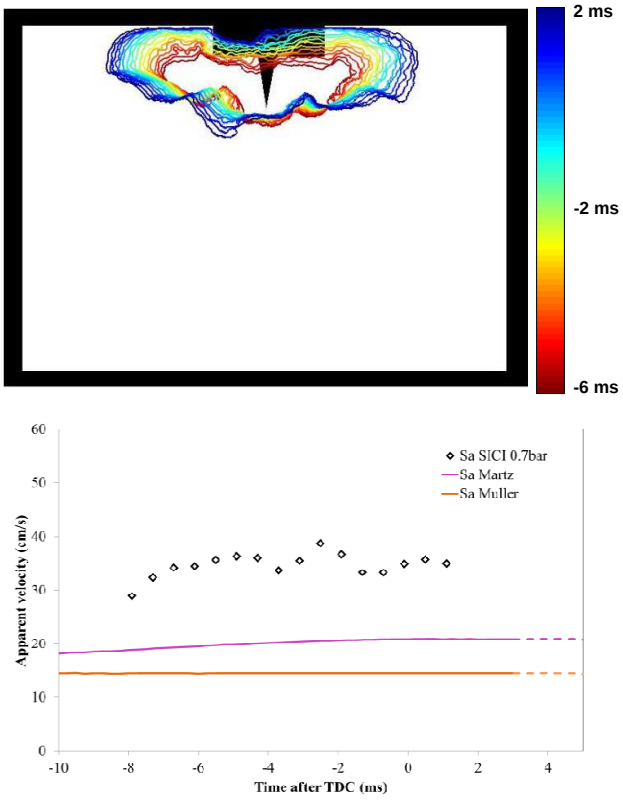

Figure 14: a) Contours of chemiluminescence at early stages of SICI combustion, P_{TDC} = 20.3 bar, configuration A. b) Apparent velocities S_a obtained from measured contours and correlations. Post-processing of contours and velocitiy are performed at 2000 fps (subsampling). See the electronic version for colors.

Figure 14-b displays the apparent velocity obtained at different instants corresponding to the early stages of the SICI combustion process. The values obtained few milliseconds after the occurrence of the discharge are not reported: at these instants, the emission from the flame is weak and contour detection is more difficult. Furthermore, the obtained velocity values are fairly dependent on the threshold detection method. On the contrary, a period of 10 ms close to the Top Dead Center (TDC) is adequate for the apparent velocity post-processing: the higher pressure and temperature levels result in more intense chemiluminescence emissions. Moreover, the flame front features a smooth shape at these instants, which is also confirmed by the PLIF measurements.

Figure 14-b shows the apparent velocity is stabilized around 35 cm/s over this period. This value is

found independent of the threshold detection method. A second experiment was post-processed in the same conditions, leading to a close value over the same period. It can be noticed these data are obtained before the onset of the cool flame. Therefore the reported value of apparent velocity is not expected to be affected by pre-reactions at these instants. This can be the case later, but values of S_a obtained from the contours are not retained because of the three dimensional shape of the flame front induced by the corner vortices.

Figure 14-b also reports the velocities obtained from the correlation of Martz *et al.* [50]. It was established from 1D unsteady simulations of laminar flame propagations using detailed chemistry. The correlation was developed for SICI combustion of isooctane – air mixtures over a wide range of temperature and equivalence ratios ($300 < T_0 < 1000$ K, $0.3 \leq \Phi \leq 1$). Following the approach of Martz et al. [50], the concept of flame burning velocity is employed in the following: it can be considered as valid provided that the instant under consideration is not too close to the auto-ignition event [50].

From a practical point of view, burning velocities obtained from the correlation are based on the measured pressure and an estimate of the unburned temperature. The latter is computed by a zero dimensional two-zones thermodynamic model similar to that of Saray *et al.* [51]. Heat capacities are obtained from Gaseq [52] and a value equal to 44.4 MJ/kg is employed for the lower calorific value of iso-octane. The model is fitted to agree both with the pressure traces measured within the RCM and with the volume of the vessel measured at TDC. Velocities obtained from the correlation of Müller *et al.*[53] are reported as well, by using the same model for estimating the unburned temperature. This correlation was published prior to that of Martz et al. [50] using a numerical approach as well. It covers the following range of conditions: $300 < T_0 < 800$ K, $0.6 \leq \Phi \leq 1$. Consequently, it is less suited to the very lean conditions under consideration here. These two correlations provide burning velocities S_u, e.g. the velocity of the reaction front in the frame of reference of unburned mixture. For the sake of comparison with our experimental data, the results of the correlations reported in Fig. 14 are multiplied by a factor ρ_u/ρ_b., where ρ_u and ρ_b are the densities in the unburned and burned mixture. This leads to the apparent flame velocity S_a – a

quantity often called S_b [50] - for an equivalent one dimensional unstreched flame. Figure 14 shows the magnitude orders obtained from both correlations are consistent with the measurements. Nevertheless, that of Martz *et al.* [50] under-predicts the velocity near TDC by a factor nearly equal to two. A factor 2.5 is obtained from Müller *et al.* [53], this one being less adapted for the very lean mixture under consideration. The imperfect match of the present SICI results with correlations was expected as such an accurate comparison relies on hypotheses, discussed in [10]: for instance, effects of flame stretch are neglected as well as the influence of residual flow. In particular, the direction of the unburned gases velocity should be normal to the flame front. Nevertheless, the relative agreement reported in Fig. 14 at early stages of SICI experiments is sufficient to confirm the observed mode of combustion is representative of deflagrations.

4.3 Propagation of reactive fronts: HCCI experiments

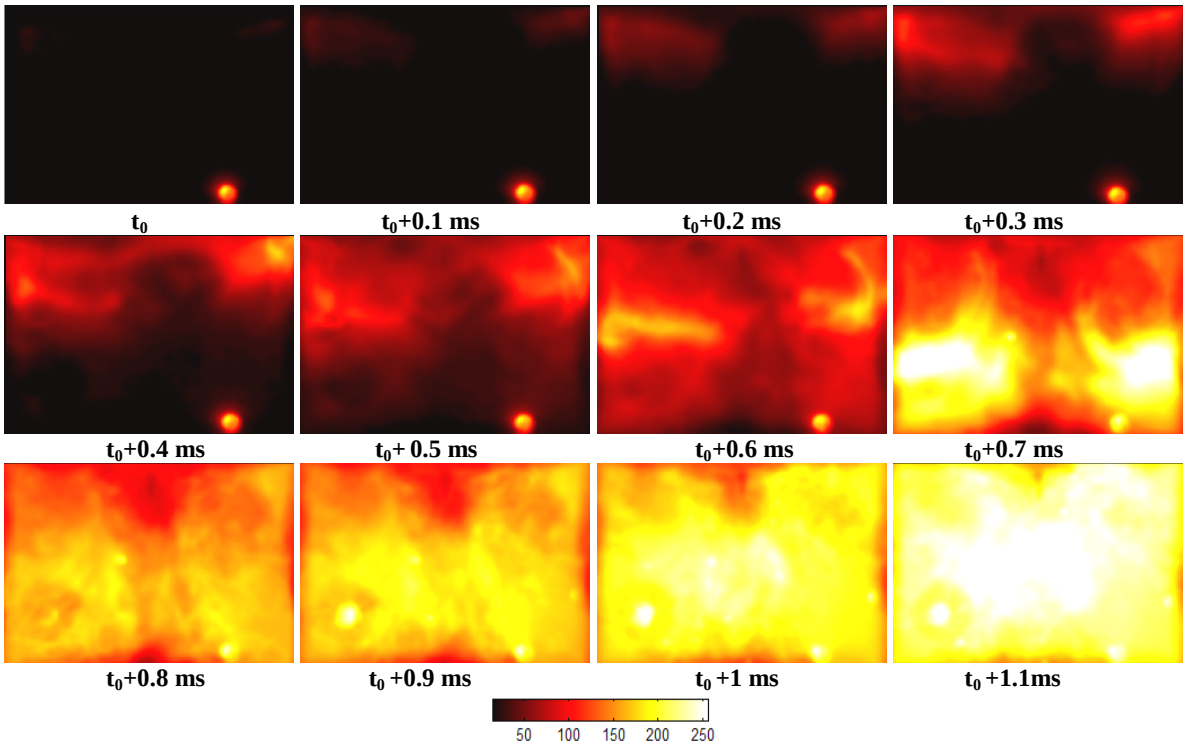

Figure 15: Chemiluminescence images obtained at the onset of hot ignition during HCCI combustion. Iso-octane – air mixture at $\Phi = 0.5$, $P_{TDC} = 26.9$ bar. Optical configuration A.

In the investigated HCCI conditions, chemiluminescence emission is only detected during hot ignition. Hence apparent velocities are estimated during this period with the same method as previously. Figure 15 reports the corresponding images recorded at the onset of auto-ignition stage for short ignition delays at 20000 frames per second with the fast camera SA5 (optical

configuration A). At the onset of hot ignition, two kernels appear near the corners of the cylinder head. After that, they grow concentrically. This period is retained for the estimation of apparent propagation velocities as the ellipsoidal shape of the fronts is more appropriate for the post-processing and for the subsequent analysis: it is concave towards the burned gases. Ignition kernels merge 0.25 ms after the first image of chemiluminescence. Afterwards, contours suggest a vertical propagation towards the piston and then chemiluminescence is detected in the whole visualization zone. It is recalled that the shape of the flame front at these instants is complex and three dimensional effects cannot be fully captured by chemiluminescence, as evidenced in section 3 by PLIF images. For the same reasons, information provided in Fig. 15 at the end of the auto-ignition process is qualitative. It is fairly similar to that already discussed previously for auto-ignition stage of SICI combustion: auto-ignition occurs near the lateral walls and then in the middle of the chamber. The difference is that in the SICI case, autoignition occurs near the piston since the flame already burned the mixture near the cylinder head.

Figure 16-a displays the contours of chemiluminescence emissions recorded at the beginning of hot ignition. The corresponding apparent velocities are reported in Fig. 16-b. The values are stabilized at about 2500 cm/s at these instants. From a more qualitative point of view, it is recalled faster apparent propagations are suggested by chemiluminescence images at late stages of auto-ignition, see Fig. 16-a. The values of about 2500 cm/s are two magnitude orders higher than that provided by the correlations, despite they account for the pressure increase resulting from the cool flame. Such values are incompatible with the laminar deflagration regime characteristic of these correlations. Furthermore much lower front velocities are obtained during the flame propagation at the early stages of SICI combustion process, in spite of the more vigorous residual aerodynamics at this instant. Therefore such high velocities are not attributed to a turbulent deflagration mode. Furthermore, the front propagation is not significantly affected by eventual small scale velocity fluctuations at this instant as fairly smooth contours are obtained by PLIF at the onset of hot ignition - at t= 18.36 ms - in the HCCI mode considered here. For these reasons, the high velocity levels are interpreted as the result of the propagation of spontaneous auto-ignition fronts. Such

regimes were already observed about 10 ms after TDC with the same device with a stoichiometric methane-air mixture, as a result of the weak thermal gradients in the hot zone shortly after TDC [8]. The same regime is obtained here for a hydrocarbon featuring very different ignition behavior, e.g. two-stage instead of single stage ignition. Such fast propagation regimes were also reported in engines, e.g. in fully turbulent configurations: the global apparent velocity reaches up to 8200 cm/s in the work of Hultqvist *et al.* by cycle resolved fuel tracer PLIF [21] in HCCI mode. Schließl *et al.* [54] reported a value of 2500 cm/s during end-gas self-ignition in a SI engine. Bladh et al. [55] reported values of 1000-2000 cm/s in similar conditions by using double pulse 355 nm PLIF, but they correspond to the turbulent flame propagation in the end-gas, and not to the auto-ignition process. Therefore our measurements should only be compared to that reported in [21, 54].

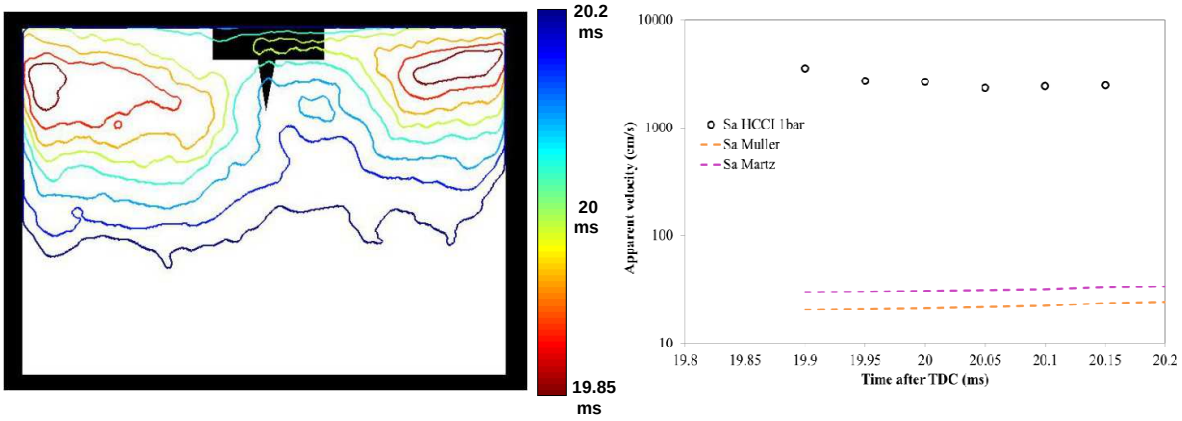

Figure 16: a) Contours of chemiluminescence at the onset of hot ignition during HCCI combustion. Short ignition delays, P_{TDC} = 26.9 ms. Optical configuration A. b) Apparent velocities S_a obtained from contours and correlations. Post-processing of contours and velocity performed at 20000 fps. See the electronic version for colors.

4.4 HCCI at long ignition delays

HCCI experiments with long ignition delay (P_{TDC} = 19.6 bar) and with optical configuration B are analyzed herein. Several ignition kernels are depicted in chemiluminescence images, as shown by iso-contours reported in Fig. 17. Apparent velocities of about 1 m/s are obtained. The magnitude order is representative of a deflagration, but it is several times higher than the value obtained from Müller al al. [52] with the previously evoked approach. The value is also more than the double of the SICI case, see Fig. 14, which suggests apparent velocities may be enhanced by pre-reacted mixture composition close to auto-ignition conditions. Such a behavior was reported in the literature, see for instance [45] for similar lean iso-octane air mixtures, at higher temperatures.

Double-pulse 355 nm PLIF images were obtained few milliseconds later, at 65.59 ms and 67.59 ms in the same conditions, see Fig 10. The apparent velocity computed from these PLIF measurements with the same procedure as previously for chemiluminescence is equal to 76.1 cm/s. This value is relatively close to that obtained by chemiluminescence 63 ms after TDC, see Fig.17b, which confirms the deflagrative nature of the combustion process: a transition from auto-ignition to deflagration occurs at the beginning of the second stage of ignition, as evoked in § 3.1.4. Curvature of the flame front at intermediate scales is observed, suggesting a wrinkled flame combustion regime is reached at these late instants. These results provide interesting insight about the nature of the combustion process for HCCI combustion. In particular, long ignition delays are often measured in RCMs with flat piston, and the present work highlight the influence of flat piston aerodynamics through temperature distribution and turbulence. The former is responsible for multiple auto-ignition kernels and for the transition to deflagration, while turbulence affects the subsequent flame propagation and thus the global burning rate.

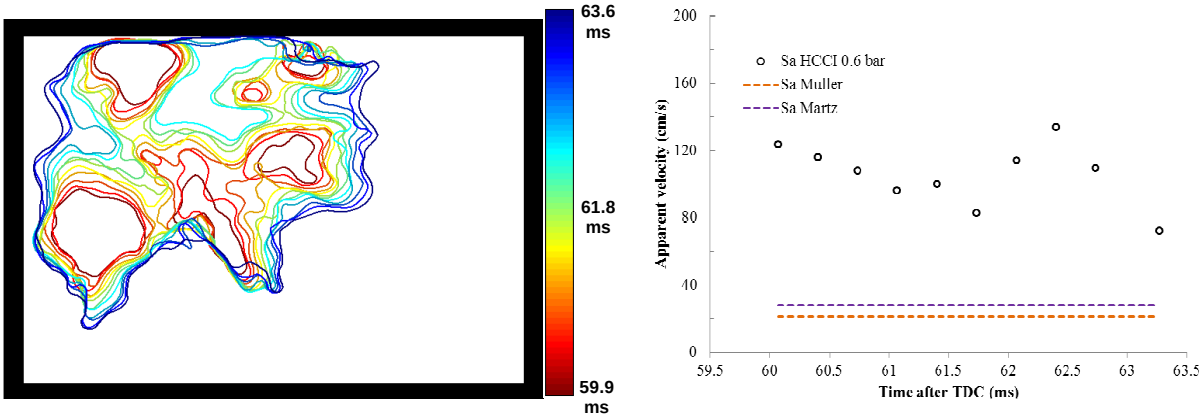

Figure 17: a) Contours of chemiluminescence at the onset of hot ignition during long ignition delay HCCI combustion. P_{TDC} = 19.6 bar, Optical configuration B. b) Apparent velocities S_a obtained from measured contours and correlations. Contours and velocitiy post-processings correspond to 3000 fps.
See the electronic version for colors.

5. Conclusion

Homogeneous Charge Compression Ignition (HCCI) and Spark Induced Compression Ignition (SICI) of a lean iso-octane air mixture are investigated through simultaneous measurements of planar laser-induced fluorescence at 355 nm and high-speed chemiluminescence in the parallelepipedic combustion vessel of a rapid compression machine (RCM). The fluorescence

images show the presence of intermediate species produced during the cool flame with a significant contribution of formaldehyde. These species are consumed at the high temperatures characteristic of either hot ignition or flame propagation. This two dimensional diagnostic method brings useful information about the location and shape of reactive fronts, and is efficient until the latest instants of combustion.

By contrast, high-speed chemiluminescence enables time resolved investigation of these reactive fronts with spatial integration along the combustion chamber depth. Furthermore, the first ignition kernels can be detected as the full volume of the chamber is visualized after TDC. The coupling of these two diagnostics provides complementary information about the transient three dimensional combustion processes.

Phenomenology of HCCI combustion is investigated by these means: original results were reported through temporal evolution of PLIF images during the first stage of ignition. They put into evidence the first reactive phenomena are driven by the effect of thermal stratification on cool flame pre-reactions: initiated in the hot zone, the cool flame then propagates within the initially colder region. For short ignition delays, fast consumption of formaldehyde is observed during the second stage of ignition. It is associated with a steep pressure rise. For long ignition delays, relatively slow propagation of wrinkled reactive fronts is reported along with a smooth pressure rise. In agreement with previous studies, the rate of pressure rise, e.g. the heat release rate, is strongly correlated to the local mode of combustion: deflagration or auto-ignition fronts. This combustion mode depends on the ignition delay, as the pre-ignition temperature field results from the unsteady large scale aerodynamics and turbulent mixing. Finally, RCM is found to be an interesting tool to analyze HCCI combustion mode for lean mixtures featuring a low fluctuations levels of ignition delays. In particular, the combustion process and the related temperature distribution observed for long ignition delays present some similarities with those encountered within engines. By contrast, the existence of hot zones at TDC with very low gradients is more specific to RCMs and affects the combustion process for short ignition delays. However, the front velocities are representative of practical applications, and finally this provides a unique opportunity to study auto-ignition front

phenomena with a temperature distribution which is well controlled and more academic than in HCCI engines.

The combined diagnostics provide as well essential information for the phenomenological analysis of SICI combustion in severe conditions, e.g. for a very lean mixture at high pressure. A high ignition energy level of 305 mJ was required for the flame kernel to resist to post-compression conditions, and in particular to the induced aerodynamics. This value was also chosen to obtain a significant decrease in the auto-ignition delays of the end gas. This makes the specificity of the investigated SICI conditions. The interaction between three phenomena is put into evidence in these conditions: (i) the flame consumes a pre-reacted gaseous mixture, (ii) the flame front, initially laminar, is highly affected by the large-scale post-compression aerodynamics and in particular by corner vortices, and (iii) it becomes progressively wrinkled by turbulence. Such phenomena influence the flame surface and its propagation velocity, and consequently the heat release rate, which is a key parameter for these combustion modes. As evoked above, flame propagation is followed by the auto-ignition of the end gas. In comparison to HCCI results, SICI experiments feature lower maximum values of the rate of pressure rise, for similar ignition delay values. This tends to illustrate the relevance of SICI combustion for practical applications. Large zones of formaldehyde disappear near the piston at the end of combustion process, and fast motions of light emission are detected on chemiluminescence records. This confirms the occurrence of fast auto-ignition fronts at the last stage of SICI combustion process, which is in agreement with the relatively high value of the recorded rate of pressure rise at these instants. In the HCCI case for short ignition delays, e.g. for a similar auto-ignition timing, fast fronts also propagate, leading to a higher rate of pressure rise. They propagate in a large zone initially located at the top of the chamber. These results suggest thermal gradients and their distribution in space represent a mean to control both the auto-ignition front velocity, and their area surface and thus heat release rate at the end of the SICI process, whereas the chemical composition, pressure and temperature significantly affect all the different stages of the SICI process. From a more quantitative point of view, the cycle resolved analysis of reactive fronts by chemiluminescence enables estimating an apparent velocity

at early stages of propagation. The obtained values confirm the existence of two propagative modes, namely deflagration and auto-ignition in the HCCI cases at these instants. Double-pulse 355 nm PLIF images confirm the propagation velocities are representative of deflagrations in the measurement plane at large ignition delays values in the HCCI case. In conditions similar to the SICI case, this double frame diagnostic confirms the existence of fast autoignition processes during hot ignition of the end gas. It suggests the presence of a more volumetric – but subsonic - consumption process, which is fairly different from the fast auto-ignition front propagating in HCCI mode for short ignition delays.

The gathered data are relevant for future assessments of combustion models for the simulation of HCCI/SICI combustion modes in lean conditions, and in particular in the presence of heterogeneities. In future works, the phenomenology described here may be useful as well for the analysis of a larger experimental database devoted to SICI combustion. In addition, the proposed double pulse formaldehyde PLIF technique coupled to fast chemiluminescence was found relevant to study the late stages of the combustion process, when complex three dimensional effects occur. Such a time resolved planar diagnostic technique will be relevant for further parametric studies of the fast dynamics of auto-ignition fronts at these instants.

Acknowledgements

The authors are grateful to RENAULT for financial support, and particularly wish to thank A. Agneray for his scientific collaboration to this work. Francisco Ronchi is acknowledged for his participation to the experiments.

References

[1] M. Yao, Z. Zheng, H. Liu, Progress and recent trends in homogeneous charge compression ignition (HCCI) engines. Prog. Energ. Combust. Sci. 35 (2009) 398-437.

[2] G.A. Lavoie, J.B. Martz, M.S. Wooldridge, D. Assanis, A Multi-Mode Combustion Diagram for Spark Assisted Compression Ignition. Combust. Flame 157 (2010) 1106-1110.

[3] J.B. Martz, Simulation and model development for auto-ignition and reaction front propagation in low-temperature high-pressure lean-burn engines, Ph.D. Thesis, University of Michigan, 2010.

[4] B. Zigler, An Experimental investigation of the properties of low temperature combustion in an optical engine, Ph.D. Thesis, University of Michigan, 2008.

[5] A. K. Agarwal, A. P. Singh, R. K. Maurya, Evolution, challenges and path forward for low temperature combustion engines, Prog. Energ. Combust. Sci. 61 (2017) 1-56.

[6] A. Cavaliere, M. D. Joannon, Mild Combustion, Prog. Energ. Combust Sci. 30 (2004) 329–366.

[7] Z. Wang, X. He, J.X. Wang, S. Shuai, F. Xu, D. Yang, Combustion visualization and experimental study on spark induced compression ignition (SICI) in gasoline HCCI engines, Energ. Conver. Manage. 51 (2010) 908-917.

[8] G. Mittal, C.J. Sung, Aerodynamics inside a rapid compression machine. Combust. Flame, 145 (2006) 160-180.

[9] C. Strozzi, J. Sotton, A. Mura, M. Bellenoue, Characterization of a two-dimensional temperature field within a rapid compression machine using a toluene planar laser-induced fluorescence imaging technique, Meas. Sci. Technol. 20 (2009) 1-13.

[10] C. Strozzi, A. Mura, J. Sotton, M. Bellenoue, Experimental analysis of propagation regimes during the autoignition of a fully premixed methane–air mixture in the presence of temperature inhomogeneities, Combust. Flame 159 (2012) 3323-3341.

[11] M. Ben Houidi, J. Sotton, M. Bellenoue, Interpretation of auto-ignition delays from RCM in the presence of temperature heterogeneities: Impact on combustion regimes and negative temperature coefficient behavior, Fuel 186 (2016) 476–495.

[12] S.M. Walton, X. He, B.T. Zigler, M.S. Wooldridge, A. Atreya, An experimental investigation of iso-octane ignition phenomena, Combust. Flame 150 (2007) 246-262.

[13] A.B. Mansfield, M.S. Wooldridge, High-pressure low-temperature ignition behavior of syngas mixtures, Combust. Flame 161 (2014) 2242-2251.

[14] K.P. Grogan, S.S. Goldsborough, M. Ihme, Ignition regimes in rapid compression machines, Combust. Flame 162 (2015) 3071-3080.

[15] H.G. Im, P. Pal, M.S. Wooldridge, A.B. Mansfield, A regime diagram of homogeneous reactant mixtures with turbulent velocity and temperature fluctuations, Combust. Sci. Technol. 187 (2015) 1263–1275.

[16] M.A. Boumehdi, S.A. Stepanyan, P. Desgroux, G. Vanhove, S.M. Starikovskaia, Ignition of methane- and n-butane-containing mixtures at high pressures by pulsed nanosecond discharge, Combustion and Flame 162 (2015) 1336–1349.

[17] J.E. Harrington, K.C. Smyth, Laser-induced fluorescence measurements of formaldehyde in a methane/air diffusion flame, Chem.Phys. Letter 202 (1993) 196-202.

[18] C. Brackmann, J. Nygren, X. Bai , Z. Li, H. Bladh, B. Axelsson, I. Denbratt, L. Koopmans, P.-E. Bengtsson, M. Aldén, Laser-induced fluorescence of formaldehyde in combustion using third harmonic Nd:YAG laser excitation, Spectrochim. Acta A Mol. Biomol. Spectrosc. 59 (2003) 3347-56.

[19] R. Collin, J. Nygren, M. Richter, M. Aldén, L. Hildingsson, B. Johansson, Simultaneous OH and formaldehyde-LIF measurements in an HCCI engine, (2003) SAE paper 2003-01-3218.

[20] T. Kim, J.B. Gandhi, Investigation of light load HCCI combustion using formaldehyde using planar laser induced fluorescence. Proc. Combust. Inst. 30 (2005) 2675-2682.

[21] A. Hultqvist, M. Christensen, B. Johansson, A. Franke, A Study of the Homogeneous Charge Compression Ignition Combustion Process by Chemiluminescence Imaging. (1999) SAE Technical Paper 1999-01-3680.

[22] J. Kashdan, G. Bruneaux, Mixture Preparation and Combustion in an Optically-Accessible HCCI, Diesel Engine, Oil Gas Sci. Technol. 61 (2006) 25-42.

[23] A. Fayoux, K. Zähringer, O. Gicquel, J.C. Rolon, Experimental and numerical determination of heat release in counterflow premixed laminar flames, Proc. Combust. Inst. 30 (2005) 251–257.

[24] C. Strozzi, J. Sotton, A. Mura, M. Bellenoue, Experimental and numerical study of the influence of temperature heterogeneities on self-ignition process of methane-air mixtures in a rapid compression machine. Combust. Sci. Technol., 180 (2008) 1829-1857.

[25] V. Prevost, Autoinflammation de mélanges pauvres assistée par plasma. PhD Thesis, Ecole Nationale Supérieure de Mécanique et d'Aérotechnique, 2013.

[26] N. Maes, M. Meijer, N. Dam, B. Somers, H. B. Toda, G. Bruneaux, S. A. Skeen, L.M. Pickett, J. Manin, Characterization of Spray A flame structure for parametric variations in ECN constant-volume vessels using chemiluminescence and laser-induced fluorescence, Combust. Flame 174 (2016) 138–151.

[27] S. A. Skeen, J. Manin, L.M. Pickett, Simultaneous formaldehyde PLIF and high-speed schlieren imaging for ignition visualization in high-pressure spray flames, Proc. Combust. Inst. 35 (2015) 3167–3174.

[28] J. Oloffson, H. Seyfried, M. Richter, M. Aldén, A. Vressner, A. Hultqvist, B. Johansson, K. Lombaert, High-speed LIF Imaging for cycle-resolved formaldehyde visualization in HCCI combustion, SAE technical paper series, SAE 2005-01-0641.

[29] Q. Tang, H. Liu, M. Li, M. Yao, Z. Li, Study on ignition and flame development in gasoline partially premixed combustion using multiple optical diagnostics, Combust. Flame, 177 (2017) 98-108.

[30] M. Ben Houidi, J. Sotton, A. Claverie, C. Strozzi, M. Bellenoue, Application of high-speed PIV and Toluene PLIF techniques to study aerodynamics and thermal stratification inside a flat piston Rapid Compression Machine, 18th International Symposium on the Application of Laser and Imaging Techniques to Fluid Mechanics (2016), Lisbon, Portugal.

[31] M. Ben Houidi, J. Sotton, M. Bellenoue, C. Strozzi, Effects of low temperature heat release on the aerodynamics of a flat piston rapid compression machine: impact on velocity and temperature fields, 37th International Symposium on Combustion (2018), Dublin, Ireland, submitted to Proc. Combust. Inst.

[32] J.-F. Griffiths, B.-J. Whitaker, Thermokinetic interactions leading to knock during Homogeneous Charge Compression Ignition. Combust. Flame, 131 (2002) 386–399.

[33] C. Strozzi, A. Delicourt, M. Bellenoue, J. Sotton, High Speed PIV Analysis of the Combustion Regimes During Autoignition of Homogeneous Fuel - Air Mixtures in a RCM. 26th ICDERS (2017), Boston.

[34] C. Strozzi, Etude expérimentale de l'auto-inflammation de mélanges gazeux en milieux confinés et sa modélisation avec une description cinétique chimique detaillée, Ph.D. Thesis, University of Poitiers, 2008.

[35] H. Quintens, M. Bellenoue, C. Strozzi, R. Zitoun, Deflagration/auto-ignition/detonation transition induced by flame propagation in a n-decane/O_2/Ar mixture, INCA Colloquium, 17-18 october. 2017, submitted to Flow Turbulence and Combustion.

[36] R.N. Dahms, G.A. Paczko, S.A. Skeen, L.M. Pickett, Understanding the ignition mechanism of high-pressure spray flames, Proc. Combust. Inst. 36 (2017) 2615-2623.

[37] A. Krisman, E.R. Hawkes, J.H. Chen, A parametric study of ignition dynamics at ECN spray A thermochemical conditions using 2D DNS, 37th International Symposium on Combustion (2018), Dublin, Ireland, submitted to Proc. Combust. Inst.

[38] J.-O. Olsson, P. Tunestål, B. Johansson, Closed-Loop Control of an HCCI Engine. SAE Technical Paper 2001-01-1031, 2001.

[39] C. J. Chiang, A. G. Stefanopoulou, Dynamics of Homogeneous Charge Compression Ignition (HCCI) Engines with High Dilution, Proceedings of the 2007 American Control Conference, DOI: 10.1109/ACC.2007.4282274.

[40] S. Saxena, I. D. Bedoya, Fundamental phenomena affecting low temperature combustion and HCCI engines, high load limits and strategies for extending these limits, Prog. Energ. Combust. Sci. 39 (2013) 457-488.

[41] A. Mariani, F. Foucher, Radio frequency spark plug: An ignition system for modern internal combustion engines, Appl. Energ. 122 (2014) 151–161.

[42] P. Flasinska, M. Fraczak, T. Piotrowski, Explosion hazard evaluation and determination of the explosion parameters for selected hydrocarbons C6 – C8, Cent. Eur. J. Energ. Mater., 9 (2012) 399-409.

[43] M.D. Kurtz, J.D. Regele, Acoustic timescale characterisation of a one-dimensional model of hot spot, Combust. Theor. Model. 18 (2014) 532-551.

[44] Y.-B. Zel'dovich, Regime classification of an exothermic reaction with nonuniform initial conditions, Combust. Flame 39 (1980) 211–214.

[45] J. Martz, G. Lavoie, H. Im, R Middleton, A. Babajimopoulos, D. Assanis, The propagation of a laminar reaction front during end-gas auto-ignition, Combust. Flame 159 (2012) 2077.

[46] J. Sidey, E. Mastorakos, R.L. Gordon, Simulations of Autoignition and Laminar Premixed Flames in Methane/Air Mixtures Diluted with Hot Products, Combust. Sci. Technol. 186 (2014) 453-465.

[47] R. Schließl, U. Maas, Analysis of endgas temperature fluctuations in an SI engine by laser-induced fluorescence, Combust. Flame 133 (2003) 19–27.

[48] G. Grieg, O. Kubler, R. Kikinis, and F. A. Jolesz., Nonlinear Anisotropic Filtering of MRI Data. IEEE Transactions on Medical Imaging, 11 (1992) 221-232.

[49] N. Otsu, A Threshold Selection Method from Gray-Level Histograms, IEEE Transactions on Systems, Man, and Cybernetics, 9 (1979) 62-66.

[50] J.-B. Martz, R.-J. Middleton, G.-A. Lavoie, A. Babajimopoulos, D.-N. Assanis, A computational study and correlation of premixed isooctane–air laminar reaction front properties under spark ignited and spark assisted compression ignition engine conditions. Combust. Flame 158 (2011) 1089–1096.

[51] R.-K. Saray, M. Fathi, M.-D. Checkel, Detailed Approach for Apparent Heat Release Analysis in HCCI Engines, Fuel 89 (2010) 2323-2330.

[52] GASEQ, a chemical equilibrium program for Windows, v0.79, www.gaseq.co.uk.

[53] U.-C. Muller, M. Bollig, N. Peters, Approximations for burning velocities and Markstein numbers for lean hydrocarbon and methanol flames. Combust. Flame 108 (1997) 349-356.

[54] R. Schließl, A. Dreizler, U. Maas, A.-J. Grant, P. Ewart, Double-Pulse PLIF Imaging of Self-Ignition Centers in an SI Engine, (2001) SAE2001-01-1925.

[55] H. Bladh, C. Brackmann, P. Dahlander, I. Denbratt, P-E Bengtsson. Flame propagation visualization in a spark-ignition engine using laser-induced fluorescence of cool-flame species. Meas. Sci. Technol. 16 (2005), 1083-1091.